Fig. 9. NCC derivatives were mislocalized in *Shh* mutant embryos in areas where *Ptch1*^{LacZ} was normally expressed. The NCC marker *Ap2α* expressed in the dorsal neural tube and DRGs (A) was expanded into the ventral neural tube as well as across the midline below the neural tube (C vs. B). e11.5 sections of NCC trace compared to *Ptch1*^{LacZ} showed the DRG axons abnormally crossing the midline in *Shh* mutants (F vs. E) where *Ptch1*^{LacZ} is normally expressed (D). In addition, the DRGs were fused in the midline as predicted by *Ap2α* expression (arrows I vs. H). However, these defects are not restricted to the ventral neural tube area as the DRGs were also fused in the A–P axis (I vs. H arrowheads) where *Ptch1*^{LacZ} also had a segmental pattern (G). This fusion was consistent with the neuronal staining of cranial nerves and DRGs (Figs. 4J–M). Lineage traced NCCs were also abnormally seen in the dorsal pharyngeal region and midline of *Shh*$^{-/-}$ embryos (arrows L vs. K) as well as the OT of the heart (Fig. 7), all corresponding with areas of normal *Ptch1*^{LacZ} expression. These data strongly suggest that NCC derivatives are mislocalized in *Shh*$^{-/-}$ embryos. O—otocyst, P—pharynx, AS—aortic sac.

significantly on NCCs between e9.5–11.5. Bmp signaling has been implicated in the early development of NCCs (Aybar et al., 2002; Baker and Bronner-Fraser, 1997). We therefore examined for changes in Bmp expression in *Shh*$^{-/-}$ embryos. Significantly, we noted a marked reduction in *Bmp4* expression in the dorsal ectoderm of *Shh* mutant embryos. This change in Bmp expression might explain early loss of NCCs. However, lineage tracing of NCCs revealed significant loss within the arches also, consistent with later morphological defects seen in *Shh*$^{-/-}$ embryos. Analysis of cell death revealed a striking pattern

of apoptosis of NCCs and pharyngeal endoderm within the arches. Examination of four NCC markers, *Crabp1*, *Ap2α*, *Twist*, and *Sox9*, revealed significant differences in patterns of expression. While *Crabp1*, *Twist*, and *Sox9* were absent from the first arch, *Ap2α* continued to be expressed within the arch ectoderm (Fig. 10 and data not shown). In addition, *Sox9* expression was absent or reduced in several significant places including the distal pharyngeal arches and the developing DRGs and/or somites (Figs. 10C,D). Strikingly, the loss of *Sox9* at e9.5 and 10.5 matched the pattern of apoptosis seen in three-dimensional reconstructions of cell death in *Shh*$^{-/-}$ embryos (Fig. 10I). This also correlated with the areas where NCCs were missing in the arches and the DRGs as determined by NCC lineage tracing (Figs. 10G,H and data not shown). While this loss of expression may represent dead cells, the continued expression of *Ap2α* in the same cells, both mRNA and protein (data not shown), suggests that maintenance of *Sox9* expression in NCCs is lost in *Shh*$^{-/-}$ embryos, possibly resulting in their death.

Discussion

Shh$^{-/-}$ embryos demonstrate a developmental mechanism for pulmonary artery atresia

Evaluation of *Shh*$^{-/-}$ embryos near term revealed a single OT arising from both ventricles. This conformation is suggestive of conotruncal septation failure. However, OT development in *Shh*$^{-/-}$ embryos is abnormal prior to the onset of septation with clear absence of the forming pulmonary artery (Figs. 3A–H). Our results suggest that the pulmonary artery fails to form in *Shh*$^{-/-}$ embryos, not because of a failure of conotruncal septation, but rather due to hypoplasia of the caudal ventral pharynx and failure to form the fourth and sixth aortic arch arteries. In addition, shortening of the OT may contribute to the abnormal pulmonary artery development. Loss of these structures appears to result in a failure to maintain the endothelial channel that normally forms the pulmonary artery. The third arch artery then presumably compensates for the loss of the fourth arch artery to become the aortic arch and maintain the cardiac circulation. Our data also suggest that mislocalization of NCCs within the OT channel may partially obstruct the pulmonary channel, possibly contributing to the observed phenotype. While the etiology of the agenesis of the fourth and sixth arches (and arteries) remains unclear, extensive cell death in the pharyngeal endoderm and NCCs of the arches seems the most likely cause.

Shh, *Ihh*, and the anterior heart field

As early as e8.75, shortening of the OT can be seen in *Shh*$^{-/-}$ embryos. At this stage, *Shh*$^{-/-}$ embryos are difficult to distinguish in size and morphology from wild type
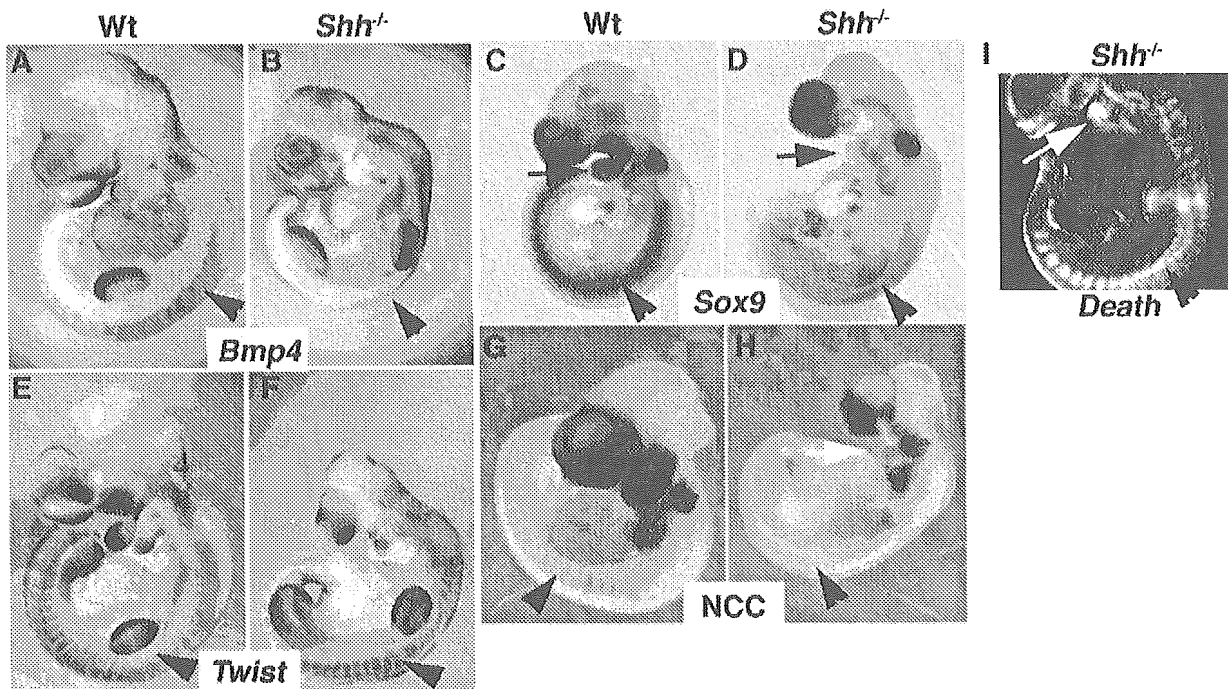
Fig. 10. Whole-mount mRNA in situ demonstrated loss of dorsal surface ectoderm expression of *Bmp4* in e10.5 *Shh* mutants (A vs. B). *Sox9* expression was abnormal as early as e9.5 in *Shh* mutants (C vs. D) and the domains of lost expression match those where NCCs are absent (G,H). There was increased cell death (I) where *Sox9* was missing in the 1st arch (arrow) and trunk (arrowheads) of similar-staged *Shh* mutant embryos (C,D,I). In addition, general somite segmentation was present as late as e10.5 in *Shh* mutants, indicating that the A–P fusion of the DRGs was not a general phenomenon (E,F arrowhead) but more specific to NCC derivatives.

embryos, suggesting that the decreased OT size is not simply due to growth retardation. The smaller OT appears to be the source of the "pulling up" of the right ventricle observed in *Shh*$^{-/-}$ embryos (Izraeli et al., 1999; Tsukui et al., 1999), a process described in manipulated chick embryos with a shortened outflow tract (Yelbuz et al., 2002, 2003). Why are the outflow tracts and right ventricle of *Shh*$^{-/-}$ embryos reduced? Recent data have demonstrated that the normal growth of the OT and right ventricle are dependent on the newly described anterior heart field (Abu-Issa et al., 2004; Cai et al., 2003; Kelly and Buckingham, 2002; Mjaatvedt et al., 2001). Interestingly, *Ihh;Shh* double null mutants or *Smo* mutants have more severe heart defects than *Shh*$^{-/-}$ embryos (Zhang et al., 2001). These defects imply that *Ihh* in combination with *Shh* are critical for early development of myocardial precursors, possibly the anterior heart field. Whether *Ihh* and/or *Shh* play some combinatorial role in the development of the anterior heart field remains to be determined.

Shh$^{-/-}$ *cardiovascular defects resemble tetralogy of Fallot*

In addition to pulmonary artery atresia, *Shh*$^{-/-}$ embryos have VSDs as well as an overriding aorta and variable ventricular hypertrophy. This constellation of cardiac phenotypes resembles a defined syndrome, tetralogy of Fallot (TOF). Complete pulmonary artery atresia with VSD is considered to be the most severe form of this syndrome

(Adams et al., 1983). Interestingly, other defects in *Shh*$^{-/-}$ embryos such as atrial septal defects, right aortic arch, atrioventricular canal, and anomalous pulmonary venous return have all been associated with pulmonary artery atresia with VSD (Bharati et al., 1975). Intriguingly, loss of the SHH receptor SMO results in loss of *Nkx2.5* expression in the mouse. In humans, the *Nkx2.5* gene has also been implicated in TOF, particularly TOF with pulmonary atresia (Goldmuntz et al., 2001; Zhang et al., 2001). This suggests that a conserved signaling pathway involving SHH induction of *Nkx2.5* may be defective in some humans with TOF like lesions.

Previously, *Shh*$^{-/-}$ mutants have been suggested to be a model for human Vacterl (Vater) association as mutants also have renal, vertebral, and anal defects (Kim et al., 2001). Indeed, TOF is a reported cardiac defect seen in Vacterl association (Garne et al., 1999). In addition, TOF, particularly with pulmonary atresia, is also highly associated with the 22q11deletion syndrome (Chessa et al., 1998; Maeda et al., 2000) In looking for human *SHH* mutations, Nanni and colleagues examined patients with a single midline incisor, a mild form of holoprosencephaly. In the 12 patients examined, two had Vacterl syndrome, and two had 22q11deletion syndrome. Strikingly, 3 of 12 were also diagnosed with TOF. While mutations in the coding region of *SHH* were not identified in these three particular patients, regulatory regions of the *Shh* gene were not examined (Nanni et al., 2001).

Recent studies examining candidate genes contained within the 22q11deletion region have implicated loss of the transcription factor *Tbx1* as causative for some of the observed phenotypes (Jerome and Papaioannou, 2001; Lindsay et al., 2001; Merscher et al., 2001; Yagi et al., 2003). We and others have shown that *Shh*$^{-/-}$ embryos have arch artery defects similar to those seen in *Tbx1* mutants and that ectopic expression of *Shh* can result in upregulation of *Tbx1*. In addition, *Tbx1* has been implicated in anterior heart field development (Hu et al., 2004; Xu et al., 2004), consistent with our data for *Shh* mutants presented here. Furthermore, *Shh* can regulate *Tbx1* expression through *Fox* family transcription factors (*Foxc2*), indicating a regulatory relationship between *Shh* and *Tbx1* (Garg et al., 2001; Yamagishi et al., 2003). Supporting this finding, Jeong et al. (2004) provide strong evidence that Hedgehog signaling in craniofacial mesenchyme also acts through multiple *Fox* gene members including *Foxc2*. Finally, *Foxc1;Foxc2* double mutants are reported to also have anterior heart field defects (T. Kume, pers. comm.).

Our data coupled with these studies suggest that defects in the *Shh* signaling pathway may account for some patients with pulmonary atresia. Patients who also have the 22q11 deletion, Vacterl syndrome, and/or mild midline forebrain/craniofacial defects would be of particular interest to study for defects in the *Shh* signaling pathway.

Shh effect on NCC appears indirect between e9.5 and 11.5

The majority of pharyngeal arch tissue is derived from migratory NCCs with contributions from endoderm, ectoderm, and paraxial/lateral plate mesoderm. NCCs are required for development of not only the aortic arch arteries and OT septation, but also for craniofacial bones, endocrine organs of the neck, auditory ossicles, sympathetic ganglia, and dorsal root ganglia. Virtually all of these structures are missing or defective in *Shh*$^{-/-}$ embryos. Within the arches, NCCs in *Shh* mutants undergo extensive aberrant cell death, primarily in the distal first and second arches. *Ptch1*^{LacZ} expression suggests SHH diffuses and signals to adjacent mesenchyme within the arches, but not directly to NCCs between e9.5 and 10.5 as *Ptch1*^{LacZ} is not coexpressed to any significant degree in lineage traced NCCs. Supporting this observation is the finding that tissue-specific deletion of *Smo* from migratory NCCs has no visible early (e8.5–10.5) phenotype on NCC derivatives (Jeong et al., 2004), while *Shh*$^{-/-}$ embryos have visible pharyngeal defects as early as e9.0. Furthermore, work with neural tube explants supports an indirect role for SHH. NCCs do not egress from the neural tube when exposed to SHH protein from all sides, an effect that is PTCH-receptor-independent (Testaz et al., 2001). This indicates that SHH signaling to NCCs during these stages is primarily indirect or occurs without induction of *Ptch1*.

Ptch1 expression suggests that Shh may function in a pathway of NCC exclusion/repulsion

One of the surprising findings in this study is the complementary expression of *Ptch1*^{LacZ} relative to NCCs between e9.5–11.5. This suggests that the Hedgehog signaling pathway may restrict the domains that NCCs can populate. Signals emanating from the ventral neural tube act to repulse and prevent DRG axons from crossing the midline (Masuda et al., 2004). In *Shh*$^{-/-}$ embryos, we see evidence of mislocalization of NCC derivatives such as the trigeminal ganglion and the DRGs, which are fused across the midline. These findings cannot simply be due to loss of midline structures as the DRGs are also fused in the rostral–caudal axis as well. The fusion of DRGs in this axis could be accounted for by the loss of somite segmentation as a physical barrier due to cell death of the developing somites. While some somite markers at these stages are absent (*Pax1* in Figs. 4E,F), *Twist* continues to be expressed in a segmental pattern, suggesting that physical segmentation remains intact at these stages (Figs. 10E,F).

Recent evidence that SHH can act as an axonal migration chemo-attractant in the floor plate adds further support for *Shh* gene signaling acting as a guidance factor (direct or indirect) of NCCs (Charron et al., 2003). Roles in both repulsion and attraction depending on target tissue have been shown for other guidance factors. Importantly, a role for *Shh* in dorsal commissural neuron repulsion has also been reported (Bourikas et al., 2005). Interestingly, this repulsion also appeared to be independent of *Ptch1* expression and was HIP (hedgehog interacting protein)-dependent. Three other studies support this model: (1) NCCs have altered cell adhesion properties and fail to migrate from neural tube explants exposed to exogenous SHH (Testaz et al., 2001). (2) SHH can also suppress retinal ganglion axon outgrowth in vitro (Trousse et al., 2001). (3) GDNF-induced migration of enteric NCCs can be inhibited by SHH protein (Fu et al., 2004). Our data in combination with these studies suggest that *Shh* gene signaling can act either directly or indirectly as a chemo-attractant or a repulsive factor depending on the developmental context.

Therefore, these data suggest that *Shh* is necessary for some secondary mediator produced from the non-NCC mesenchyme and/or endoderm which guides NCCs. Loss of this guidance information appears to result in significant loss of NCCs through cell death. This factor(s) appears to be important at both the time of delamination and during NCC migration as *Shh*$^{-/-}$ embryos have defective NCC development at both stages.

Although dorsal patterning (where NCCs are generated) is thought to essentially remain intact, we have detected abnormal dorsal specification in *Shh*$^{-/-}$ embryos. Specifically, we have found that surface ectodermal expression of *Bmp4* is absent around the dorsal neural tube (Figs. 10A,B). Tissue-specific deletion of the *Bmp receptor 1a* gene from migratory NCCs results in their loss and OT septation

defects (Stottmann et al., 2004). Interestingly, loss of the *Bmp4* inhibitor gene *Chordin* can result in a 22q11deletion syndrome-like phenotype through alterations in NCC development, suggesting that both gain and loss of Bmp signaling can negatively affect NCCs (Bachiller et al., 2003). In addition, loss of function of *Bmp4* can result in OT defects, although these appear to be direct effects on the developing heart (and possibly the anterior heart field), not related to NCCs (Liu et al., 2004).

As Bmp signaling is thought to be critical for the development of NCCs, we cannot rule out misspecification at the time of delamination. Indeed, we noted significant increased cell death in the area of delaminating NCCs in $Shh^{-/-}$ embryos (Figs. 5E–G). However, other data presented here suggest that specification and delamination are grossly normal. Marker analysis (*Ap2α* and *Crabp1*) and *P0-Cre;R26R* lineage tracing suggest that NCCs are specified and migrate into the pharyngeal arches, but either take abnormal routes or pass through tissue from which they are normally restricted and subsequently undergo apoptosis. In addition, studies in chick have demonstrated that blocking SHH function with antibody can result in NCC death after migrating from a presumably normally patterned neural tube, suggesting that *Shh* is required after specification and migration (Ahlgren and Bronner-Fraser, 1999).

Analysis of cell death revealed a striking pattern of apoptosis within the NCCs and pharyngeal endoderm. In addition, lineage tracing of NCCs revealed significant loss of NCC derivatives within the arches consistent with later morphological defects seen in $Shh^{-/-}$ embryos. Strikingly, the pattern of cell death matched the loss of *Sox9* expression in $Shh^{-/-}$ embryos and correlated with the areas where NCCs were missing (Figs. 10G,H,I, and data not shown).

Sox9 has been implicated in the differentiation but not the induction of NCCs (Cheung and Briscoe, 2003), and SHH can induce *Sox9* (Zeng et al., 2002). Heterozygous loss of *Sox9* results in bone differentiation defects including inner ear, jaw, and palate defects (Bi et al., 2001). $Sox9^{+/-}$ mouse embryos die shortly after birth from undefined causes. Tissue-specific deletion of *Sox9* in NCCs using *Wnt1-Cre* results in bone and OT cushion defects, similar to $Shh^{-/-}$ embryos but milder (Mori-Akiyama et al., 2003; Akiyama et al., 2004). Therefore, it seems likely that loss of *Shh* results in failure to maintain *Sox9* expression and other factors resulting in the NCC-associated loss of arch-derived bone structures and possible OT defects.

In summary, loss of *Shh* affects several cell populations important in pharyngeal and cardiovascular development. NCCs are specified and migrate (including into the OT) but are mislocalized and undergo apoptosis, possibly through a combination of altered Bmp signaling and loss of *Sox9* expression. SHH does not appear to signal directly to NCCs between e9.5 and e11.5 but rather appears to induce/ suppress a secondary survival/apoptotic factor. Mislocalization of NCCs may also contribute to the loss of NCCs observed. The OT septation defects are not due solely to loss

of NCCs but rather to a general failure of caudal pharyngeal development. This failure results in no formation of the fourth and sixth arch arteries and results in pulmonary artery atresia. In addition, mislocalized NCCs may act to obstruct the developing pulmonary artery. Finally, effects on OT and right ventricular development may also be in part caused by a requirement for *Shh* on anterior heart field development. The summation of these defects results in a phenotype that resembles the most severe form of TOF. Hedgehog signaling coordinates multiple aspects of cardiovascular growth and development. Determining how the NCCs, anterior heart field, and endoderm are linked in coordinating the growth and development of the cardiovascular system will be an active area of future investigation.

References

Abu-Issa, R., Smyth, G., Smoak, I., Yamamura, K., Meyers, E.N., 2002. Fgf8 is required for pharyngeal arch and cardiovascular development in the mouse. Development 129, 4613–4625.

Abu-Issa, R., Waldo, K., Kirby, M.L., 2004. Heart fields: one, two or more? Dev. Biol. 272, 281–285.

Adams, F.H., Emmanouilides, G.C., Moss, A.J., 1983. Moss' Heart Disease in Infants, Children, and Adolescents. Williams and Wilkins, Baltimore.

Ahlgren, S.C., Bronner-Fraser, M., 1999. Inhibition of Sonic hedgehog signaling in vivo results in craniofacial neural crest cell death. Curr. Biol. 9, 1304–1314.

Ahlgren, S.C., Thakur, V., Bronner-Fraser, M., 2002. Sonic hedgehog rescues cranial neural crest from cell death induced by ethanol exposure. Proc. Natl. Acad. Sci. U. S. A. 99, 10476–10481.

Akiyama, H., Chaboissier, M.C., Behringer, R.R., Rowitch, D.H., Schedl, A., Epstein, J.A., de Crombrugghe, B., 2004. Essential role of Sox9 in the pathway that controls formation of cardiac valves and septa. Proc. Natl. Acad. Sci. U. S. A. 101 (17), 6502–6507.

Aybar, M.J., Glavic, A., Mayor, R., 2002. Extracellular signals, cell interactions and transcription factors involved in the induction of the neural crest cells. Biol. Res. 35, 267–275.

Bachiller, D., Klingensmith, J., Shneyder, N., Tran, U., Anderson, R., Rossant, J., De Robertis, E.M., 2003. The role of chordin/bmp signals in mammalian pharyngeal development and DiGeorge syndrome. Development 130, 3567–3578.

Baker, C.V., Bronner-Fraser, M., 1997. The origins of the neural crest. Part I: embryonic induction. Mech. Dev. 69, 3–11.

Bharati, S., Paul, M.H., Idriss, F.S., Potkin, R.T., Lev, M., 1975. The surgical anatomy of pulmonary atresia with ventricular septal defect: pseudotruncus. J. Thorac. Cardiovasc. Surg. 69, 713–721.

Bi, W., Huang, W., Whitworth, D.J., Deng, J.M., Zhang, Z., Behringer, R.R., De Crombrugghe, B., 2001. Haploinsufficiency of sox9 results in defective cartilage primordia and premature skeletal mineralization. Proc. Natl. Acad. Sci. U. S. A. 98, 6698–6703.

Bourikas, D., Pekarik, V., Baeriswyl, T., Grunditz, A., Sadhu, R., Nardo, M., Stoeckli, E.T., 2005. Sonic hedgehog guides commissural axons along the longitudinal axis of the spinal cord. Nat. Neurosci. 8, 297–304.

Cai, C.L., Liang, X., Shi, Y., Chu, P.H., Pfaff, S.L., Chen, J., Evans, S., 2003. Isl1 identifies a cardiac progenitor population that proliferates prior to differentiation and contributes a majority of cells to the heart. Dev. Cell 5, 877–889.

Charron, F., Stein, E., Jeong, J., Mcmahon, A.P., Tessier-Lavigne, M., 2003. The morphogen Sonic hedgehog is an axonal chemoattractant that collaborates with netrin-1 in midline axon guidance. Cell 113, 11–23.

Chessa, M., Butera, G., Bonhoeffer, P., Iserin, L., Kachaner, J., Lyonnet, S., Munnich, A., Sidi, D., Bonnet, D., 1998. Relation of genotype 22q11 deletion to phenotype of pulmonary vessels in tetralogy of fallot and pulmonary atresia-ventricular septal defect. Heart 79, 186–190.

Cheung, M., Briscoe, J., 2003. Neural crest development is regulated by the transcription factor sox9. Development 130, 5681–5693.

Chiang, C., Litingtung, Y., Lee, E., Young, K.E., Corden, J.L., Westphal, H., Beachy, P.A., 1996. Cyclopia and defective axial patterning in mice lacking Sonic hedgehog gene function. Nature 383, 407–413.

Danielian, P.S., Muccino, D., Rowitch, D.H., Michael, S.K., Mcmahon, A.P., 1998. Modification of gene activity in mouse embryos in utero by a tamoxifen-inducible form of cre recombinase. Curr. Biol. 8, 1323–1326.

Dencker, L., Annerwall, E., Busch, C., Eriksson, U., 1990. Localization of specific retinoid-binding sites and expression of cellular retinoic-acid-binding protein (CRABP) in the early mouse embryo. Development 110, 343–352.

Fagman, H., Grande, M., Gritli-Linde, A., Nilsson, M., 2004. Genetic deletion of Sonic hedgehog causes hemiagenesis and ectopic development of the thyroid in mouse. Am. J. Pathol. 164, 1865–1872.

Fu, M., Lui, V.C., Sham, M.H., Pachnis, V., Tam, P.K., 2004. Sonic hedgehog regulates the proliferation, differentiation, and migration of enteric neural crest cells in gut. J. Cell Biol. 166, 673–684.

Garg, V., Yamagishi, C., Hu, T., Kathiriya, I.S., Yamagishi, H., Srivastava, D., 2001. Tbx1, a DiGeorge syndrome candidate gene, is regulated by Sonic hedgehog during pharyngeal arch development. Dev. Biol. 235, 62–73.

Game, E., Nielsen, G., Hansen, O.K., Emmertsen, K., 1999. Tetralogy of fallot. A population-based study of epidemiology, associated malformations and survival in western Denmark 1984–1992. Scand. Cardiovasc. J. 33, 45–48.

Gitler, A.D., Brown, C.B., Kochilas, L., Li, J., Epstein, J.A., 2002. Neural crest migration and mouse models of congenital heart disease. Cold Spring Harbor Symp. Quant. Biol. 67, 57–62.

Goldmuntz, E., Geiger, E., Benson, D.W., 2001. Nkx2.5 mutations in patients with tetralogy of fallot. Circulation 104, 2565–2568.

Goodrich, L.V., Milenkovic, L., Higgins, K.M., Scott, M.P., 1997. Altered neural cell fates and medulloblastoma in mouse patched mutants. Science 277, 1109–1113.

Hogan, B., 1994. Manipulating the Mouse Embryo: A Laboratory Manual. Cold Spring Harbor Laboratory Press, Plainview, NY.

Hu, T., Yamagishi, H., Maeda, J., Mcanally, J., Yamagishi, C., Srivastava, D., 2004. Tbx1 regulates fibroblast growth factors in the anterior heart field through a reinforcing autoregulatory loop involving forkhead transcription factors. Development 131, 5491–5502.

Hutson, M.R., Kirby, M.L., 2003. Neural crest and cardiovascular development: a 20-year perspective. Birth Defects Res., Part C Embryo Today 69, 2–13.

Izraeli, S., Lowe, L.A., Bertness, V.L., Good, D.J., Dorward, D.W., Kirsch, I.R., Kuehn, M.R., 1999. The Sil gene is required for mouse embryonic axial development and left–right specification. Nature 399, 691–694.

Jeong, J., Mao, J., Tenzen, T., Kottmann, A.H., Mcmahon, A.P., 2004. Hedgehog signaling in the neural crest cells regulates the patterning and growth of facial primordia. Genes Dev. 18, 937–951.

Jerome, L.A., Papaioannou, V.E., 2001. DiGeorge syndrome phenotype in mice mutant for the T-Box gene, Tbx1. Nat. Genet. 27, 286–291.

Jiang, X., Rowitch, D., Soriano, P., Mcmahon, A.P., Sucov, H., 2000. Fate of the mammalian cardiac neural crest. Development 127, 1607–1616.

Kelly, R.G., Buckingham, M.E., 2002. The anterior heart-forming field: voyage to the arterial pole of the heart. Trends Genet. 18, 210–216.

Kim, P.C., Mo, R., Hui, C., 2001. Murine models of VACTERL syndrome: role of Sonic hedgehog signaling pathway. J. Pediatr. Surg. 36, 381–384.

Kuratani, S.C., Kirby, M.L., 1992. Migration and distribution of circumpharyngeal crest cells in the chick embryo. Formation of the circumpharyngeal ridge and e/c8+ crest cells in the vertebrate head region. Anat. Rec. 234, 263–280.

Le Douarin, N.M., Dupin, E., 2003. Multipotentiality of the neural crest. Curr. Opin. Genet. Dev. 13, 529–536.

Lindsay, E.A., Vitelli, F., Su, H., Morishima, M., Huynh, T., Pramparo, T., Jurecic, V., Ogunrinu, G., Sutherland, H.F., Scambler, P.J., Bradley, A., Baldini, A., 2001. Tbx1 haploinsufficieny in the DiGeorge syndrome region causes aortic arch defects in mice. Nature 410, 97–101.

Litingtung, Y., Lei, L., Westphal, H., Chiang, C., 1998. Sonic hedgehog is essential to foregut development. Nat. Genet. 20, 58–61.

Litingtung, Y., Dahn, R.D., Li, Y., Fallon, J.F., Chiang, C., 2002. Shh and Gli3 are dispensable for limb skeleton formation but regulate digit number and identity. Nature 418, 979–983.

Liu, W., Selever, J., Wang, D., Lu, M.F., Moses, K.A., Schwartz, R.J., Martin, J.F., 2004. Bmp4 signaling is required for outflow-tract septation and branchial-arch artery remodeling. Proc. Natl. Acad. Sci. U. S. A. 101, 4489–4494.

Maeda, J., Yamagishi, H., Matsuoka, R., Ishihara, J., Tokumura, M., Fukushima, H., Ueda, H., Takahashi, E., Yoshiba, S., Kojima, Y., 2000. Frequent association of 22q11.2 deletion with tetralogy of fallot. Am. J. Med. Genet. 92, 269–272.

Maschhoff, K.L., Baldwin, H.S., 2000. Molecular determinants of neural crest migration. Am. J. Med. Genet. 97, 280–288.

Masuda, T., Fukamauchi, F., Takeda, Y., Fujisawa, H., Watanabe, K., Okado, N., Shiga, T., 2004. Developmental regulation of notochord-derived repulsion for dorsal root ganglion axons. Mol. Cell. Neurosci. 25, 217–227.

Merscher, S., Funke, B., Epstein, J.A., Heyer, J., Puech, A., Lu, M.M., Xavier, R.J., Demay, M.B., Russell, R.G., Factor, S., Tokooya, K., Jore, B.S., Lopez, M., Pandita, R.K., Lia, M., Carrion, D., Xu, H., Schorle, H., Kobler, J.B., Scambler, P., Wynshaw-Boris, A., Skoultchi, A.I., Morrow, B.E., Kucherlapati, R., 2001. Tbx1 is responsible for cardiovascular defects in Velo–Cardio–Facial/DiGeorge syndrome. Cell 104, 619–629.

Meyers, E.N., Martin, G.R., 1999. Differences in left–right axis pathways in mouse and chick: functions of FGF8 and SHH. Science 285, 403–406.

Mitchell, P., Timmons, P., Herbert, J., Rigby, P., Tijan, R., 1991. Transcription factor Ap-2 is expressed in neural crest cell lineages during mouse embryogenesis. Genes Dev. 5, 105–119.

Mjaatvedt, C.H., Nakaoka, T., Moreno-Rodriguez, R., Norris, R.A., Kern, M.J., Eisenberg, C.A., Turner, D., Markwald, R.R., 2001. The outflow tract of the heart is recruited from a novel heart-forming field. Dev. Biol. 238, 97–109.

Moore-Scott, B.A., Manley, N.R., 2005. Differential expression of Sonic hedgehog along the anterior–posterior axis regulates patterning of pharyngeal pouch endoderm and pharyngeal endoderm-derived organs. Dev. Biol. 278, 323–335.

Mori-Akiyama, Y., Akiyama, H., Rowitch, D.H., De Crombrugghe, B., 2003. Sox9 is required for determination of the chondrogenic cell

lineage in the cranial neural crest. Proc. Natl. Acad. Sci. U. S. A. 100, 9360–9365.

Nanni, L., Ming, J.E., Du, Y., Hall, R.K., Aldred, M., Bankier, A., Muenke, M., 2001. Shh mutation is associated with solitary median maxillary central incisor: a study of 13 patients and review of the literature. Am. J. Med. Genet. 102, 1–10.

Neubuser, A., Peters, H., Balling, R., Martin, G.R., 1997. Antagonistic interactions between Fgf and Bmp signaling pathways: a mechanism for positioning the sites of tooth formation. Cell 90, 247–255.

Nishibatake, M., Kirby, M.L., Van Mierop, L.H., 1987. Pathogenesis of persistent truncus arteriosus and dextroposed aorta in the chick embryo after neural crest ablation. Circulation 75, 255–264.

Nusslein-Volhard, C., Wieschaus, E., 1980. Mutations affecting segment number and polarity in *Drosophila*. Nature 287, 795–801.

Santagati, F., Rijli, F.M., 2003. Cranial neural crest and the building of the vertebrate head. Nat. Rev., Neurosci. 4, 806–818.

Schlaeger, T.M., Bartunkova, S., Lawitts, J.A., Teichmann, G., Risau, W., Deutsch, U., Sato, T.N., 1997. Uniform vascular–endothelial-cell-specific gene expression in both embryonic and adult transgenic mice. Proc. Natl. Acad. Sci. U. S. A. 94, 3058–3063.

Soriano, P., 1999. Generalized LacZ expression with the Rosa26 Cre reporter strain. Nat. Genet. 21, 70–71.

Stottmann, R.W., Choi, M., Mishina, Y., Meyers, E.N., Klingensmith, J., 2004. Bmp receptor ia is required in mammalian neural crest cells for development of the cardiac outflow tract and ventricular myocardium. Development 131, 2205–2218.

Swiatek, P.J., Gridley, T., 1993. Perinatal lethality and defects in hindbrain development in mice homozygous for a targeted mutation of the zinc finger gene Krox20. Genes Dev. 7, 2071–2084.

Testaz, S., Jarov, A., Williams, K.P., Ling, L.E., Koteliansky, V.E., Fournier-Thibault, C., Duband, J.L., 2001. Sonic hedgehog restricts adhesion and migration of neural crest cells independently of the Patched-Smoothened-Gli signaling pathway. Proc. Natl. Acad. Sci. U. S. A. 98, 12521–12526.

Trousse, F., Marti, E., Gruss, P., Torres, M., Bovolenta, P., 2001. Control of retinal ganglion cell axon growth: a new role for Sonic hedgehog. Development 128, 3927–3936.

Tsukui, T., Capdevila, J., Tamura, K., Ruiz-Lozano, P., Rodriguez-Esteban, C., Yonei-Tamura, S., Magallon, J., Chandraratna, R.A., Chien, K.,

Blumberg, B., Evans, R.M., Belmonte, J.C., 1999. Multiple left–right asymmetry defects in Shh(−/−) mutant mice unveil a convergence of the Shh and retinoic acid pathways in the control of Lefty-1. Proc. Natl. Acad. Sci. U. S. A. 96, 11376–11381.

Xu, H., Morishima, M., Wylie, J.N., Schwartz, R.J., Bruneau, B.G., Lindsay, E.A., Baldini, A., 2004. Tbx1 has a dual role in the morphogenesis of the cardiac outflow tract. Development 131, 3217–3227.

Yagi, H., Furutani, Y., Hamada, H., Sasaki, T., Asakawa, S., Minoshima, S., Ichida, F., Joo, K., Kimura, M., Imamura, S., Kamatani, N., Momma, K., Takao, A., Nakazawa, M., Shimizu, N., Matsuoka, R., 2003. Role of Tbx1 in human del22q11.2 syndrome. Lancet 362, 1366–1373.

Yamagishi, H., Maeda, J., Hu, T., Mcanally, J., Conway, S.J., Kume, T., Meyers, E.N., Yamagishi, C., Srivastava, D., 2003. Tbx1 is regulated by tissue-specific forkhead proteins through a common Sonic hedgehog-responsive enhancer. Genes Dev. 17, 269–281.

Yamauchi, Y., Abe, K., Mantani, A., Hitoshi, Y., Suzuki, M., Osuzu, F., Kuratani, S., Yamamura, K., 1999. A novel transgenic technique that allows specific marking of the neural crest cell lineage in mice. Dev. Biol. 212, 191–203.

Yelbuz, T.M., Waldo, K.L., Kumiski, D.H., Stadt, H.A., Wolfe, R.R., Leatherbury, L., Kirby, M.L., 2002. Shortened outflow tract leads to altered cardiac looping after neural crest ablation. Circulation 106, 504–510.

Yelbuz, T.M., Waldo, K.L., Zhang, X., Zdanowicz, M., Parker, J., Creazzo, T.L., Johnson, G.A., Kirby, M.L., 2003. Myocardial volume and organization are changed by failure of addition of secondary heart field myocardium to the cardiac outflow tract. Dev. Dyn. 228, 152–160.

Zeng, L., Kempf, H., Murtaugh, L.C., Sato, M.E., Lassar, A.B., 2002. Shh establishes an Nkx3.2/Sox9 autoregulatory loop that is maintained by Bmp signals to induce somitic chondrogenesis. Genes Dev. 16, 1990–2005.

Zhang, X.M., Ramalho-Santos, M., Mcmahon, A.P., 2001. Smoothened mutants reveal redundant roles for Shh and Ihh signaling including regulation of l/r symmetry by the mouse node. Cell 106, 781–792.

Zucker, R.M., Hunter III, E.S., Rogers, J.M., 1999. Apoptosis and morphology in mouse embryos by confocal laser scanning microscopy. Methods 18, 473–480.

Presence and distribution of neural crest-derived cells in the murine developing thymus and their potential for differentiation

Hidetoshi Yamazaki[1,2], Emi Sakata[2], Toshiyuki Yamane[2,3], Ayano Yanagisawa[2], Kuniya Abe[4], Ken-Ichi Yamamura[5], Shin-Ichi Hayashi[2] and Takahiro Kunisada[2,6]

[1]Division of Regenerative Medicine and Therapeutics, Department of Genetic Medicine and Regenerative Therapeutics, Institute of Regenerative Medicine and Biofunction, Tottori University Graduate School of Medical Science, Yonago 683-8503, Japan
[2]Division of Immunology, Department of Molecular and Cellular Biology, School of Life Science, Faculty of Medicine, Tottori University, Yonago 683-8503, Japan
[3]Department of Pathology, Stanford University School of Medicine, Stanford, CA 94305, USA
[4]Technology and Development Team for Mammalian Cellular Dynamics, RIKEN Tsukuba Institute, BioResource Center, Tsukuba 305-0074, Japan
[5]Division of Developmental Genetics, Institute of Molecular Embryology and Genetics, Kumamoto University, Kumamoto 862-0976, Japan
[6]Department of Tissue and Organ Development, Regeneration and Advanced Medical Science, Gifu University Graduate School of Medicine, Gifu 500-8705, Japan

Abstract

Neural crest (NC) cells are multipotent cells that can differentiate into melanocytes, neurons, glias and myofibroblasts. They migrate into the fetal thymus on embryonic day (E) 12 in mice and may participate in thymic organogenesis. Although the abnormality of migration and distribution of NC cells in the thymus results in immunodeficiency, the spatial and temporal presence of their progeny cells has not been defined in detail. In this study, we traced NC-derived cells based on the myelin protein zero gene promoter-*Cre*-mediated excision. We demonstrated that large numbers of NC-derived cells in the thymus were detected on E11.5 to E16.5 but rarely on E17.5. A colony formation assay of single thymic cells demonstrated that multipotent cells with the potential to differentiate into melanocytes, neurons and/or glias were present in the E14.5 and E15.5 but not in the E17.5 fetal thymus. Furthermore, we confirmed that these multipotent cells were NC-derived cells. Taken together, these findings imply that multipotent NC-derived cells are present in the developing thymus, but rarely in this organ at a later stage, suggesting that NC-derived cells may play roles in thymic organogenesis at an early embryonic stage.

Introduction

Neural crest (NC) cells migrate and differentiate into a variety of cell lineages such as melanocytes, neurons, glial cells, myofibroblasts, chondrocytes and osteoblasts (1–5). NC cells migrating in the pharyngeal arch are thought to participate in the organogenesis of the craniofacial area, thyroid gland, heart and thymus (6–10). The failure or aberrant migration and abnormal distribution of NC cells result in a condition known as DiGeorge syndrome. It is characterized by defective aortic arch patterning, a conotruncal heart, thymic and parathyroid aplasia/hypoplasia including immunodeficiencies and craniofacial

anomalies (11, 12). These reports suggest that NC-derived cells may contribute to thymic organogenesis. Using avian systems, Le Douarin and her colleagues proposed the participation of avian NC cells in thymic organogenesis (4, 8). Using *Wnt1-Cre* reporter mice, Jiang *et al.* reported that murine cardiac NC-derived cells were detected around the thymus (13). However, in the murine thymus, the distribution or potential for differentiation of NC-derived cells has been rarely substantiated.

The thymus is composed of three major cell lineages, i.e. hematopoietic cells (including T lymphocytes), epithelial cells

that support T lymphocyte differentiation and mesenchymal cells surrounding the thymus (6, 14, 15). Experiments using chick and quail inter-species chimeras indicate that NC-derived cells differentiate into inter-lobular and outer thymic mesenchymal cells but not into hematopoietic cells or thymic epithelial cells (7, 8). Furthermore, ablation of NC cells by the microcautery of neural folds induces thymic abnormalities that reduce the numbers of both mesenchymal and epithelial cells (16, 17).

In this study, we employed the expression of the myelin protein zero (*P0*) gene, an indicator of NC-derived cells (18–21), and we chased NC-derived cells and assessed their presence, distribution, expression of adhesion molecules and potential in the murine thymus. It has been thought that melanocyte precursors might be distinct from neuronal and glial cell precursors or lose the potential to differentiate into neuron or glial cell lineages before or soon after the initiation of NC cell migration (22–27). Therefore, the demonstration of NC-derived cells that maintain the potential to differentiate into not only melanocytes but also neurons and glial cells would indicate the presence of NC-derived cells including multipotent NC cells. To examine the potential of NC-derived cells in the thymus, we developed a colony formation assay using single thymic cells incubated in the presence of endothelin 3 (ET3). ET3 is known to promote the survival and differentiation of not only melanocytes but also glial cells in avian cultures (28–30). Using these two types of analyses, we showed that at least double- or triple-potent NC-derived cells exist during early thymogenesis, and observed a severe reduction in their number at the late embryonic stages of thymus development in mice.

Methods

Mice

Mice carrying *Cre* recombinase driven by the protein 0 (*P0*) promoter were produced as described (19), and *Rosa26R* mice were obtained from Kumamoto University (18). C57BL/6 mice were purchased from Japan Clea (Tokyo, Japan).

Determination of genotypes of transgenic mice

Genomic DNA was prepared, and transgenes were detected by use of PCR. The respective sense and anti-sense primers used for PCR were as follow—*LacZ*: 5'-GGT AGC AGA GCG GGT AAA CT-3'/5'-ATC TGA CGG GCT CCA GGA GT-3' and *Cre*: 5'-GGA CAT GTT CAG GGA TCG CCA GGC G-3'/5'-GCA TAA CCA GTG AAA CAG CAT TGC TG-3'. PCR was performed by incubation at 94°C for 4 min, followed by 35 cycles of incubation at 93°C for 1 min, 58°C for 1 min and 72°C for 1 min and a final extension at 72°C for 7 min.

Histological analysis

For detection of LacZ activity, whole embryos and tissues were fixed in PBS solution (pH 7.4) containing 2% formaldehyde (Wako), 0.2% glutaraldehyde (Wako) and 0.02% NP-40 (Sigma). After washing, samples were stained with a solution containing Bluo-Gal (GIBCO-BRL) in *N,N'*-dimethylformamide (Wako) until the desired color intensity had been obtained. For preparation of tissue sections, thymi were embedded in a polyester wax (BDH Laboratory Supplies). Sections were prepared at a 7-μm thickness, and stained with hematoxylin and eosin.

Fluorescein di-β-ᴅ-galactopyranoside loading and flow cytometric analysis

Single-cell suspensions from thymi of embryonic day (E) 12.5 to 3.5-day-old mice were prepared by digestion with collagenase D (Roche), Dispase II (Roche) and trypsin/EDTA (GIBCO-BRL). Fluorescein di-β-ᴅ-galactopyranoside (FDG) staining was carried out essentially as described (31). To reduce background fluorescence, we incubated the cells in FDG staining medium [4% fetal bovine serum (FBS; JRH)/10 nM HEPES (pH 7.3)/PBS] containing 1 mM chloroquine for 30 min at 37°C, 5% CO_2. Cells were then loaded with FDG (Molecular Probe, Eugene, OR, USA) by osmotic shock. Briefly, after the cells had been allowed to equilibrate in a water bath at 37°C for 10 min, an equal volume of pre-warmed 2 mM FDG in sterile water was rapidly mixed with the cell suspension. After exactly 2 min of incubation at 37°C, the FDG loading was stopped; and cells were suspended in ice-cold staining medium containing 10 μg ml^{-1} propidium iodide for 5 min at 4°C. Then, cells were blocked with rabbit serum, and stained with biotin-conjugated rat anti-mouse mAbs against CD45 (30-F11; BD PharMingen) and integrins α4 (P/S-2; a gift from K. Miyake, Tokyo University), α5 (5H10-27; BD PharMingen), αV (RMV-7; BD PharMingen), β1 (KMI-6; a gift from K. Miyake, Tokyo University) and β3 (2C9.G2; BD PharMingen). The stained cells were further incubated with *R*-PE-labeled streptavidin (Southern Biotech Associate, Inc.). The stained cells were analyzed by using an EPICS-XL flow cytometer (Coulter).

Induction of melanocytes from thymic cells

Single-cell suspensions from thymi of E12.5 to 3.5-day-old mice were prepared as described above. The prepared cells were inoculated into 24-well plates (Corning Costar) with ST2 stromal cells (32), and cultured in α-MEM (GIBCO-BRL) containing 10% FBS (Hyclone), supplemented with the following reagents: 10^{-7} M dexamethasone (DEX, Sigma), 40 nM human recombinant ET3 (Peptide Institute) and 1 nM BQ788, an antagonist of endothelin receptor B (ETR-B; Phoenix Pharmaceuticals, Inc.). Cultures were fed every third day by replacing the medium with 2 ml of fresh medium. After 3 weeks, the cells were harvested by treatment with 0.25% trypsin/EDTA, and the number of melanocytes was counted.

Induction of melanocytes, neurons and glias in thymic clonal cell cultures

Thymic cell suspensions from E14.5, E15.5 and E17.5 embryos were prepared as described above. Then, 1–2 × 10^5 cells were inoculated into six-well plates (Corning Costar) with ST2 stromal cells (32), and cultured in α-MEM supplemented with 10% FBS, 10^{-7} M DEX, 40 nM human ET3, 1 nM heregulin (Phoenix Pharmaceuticals, Inc.) and 1 nM forskolin (Phoenix Pharmaceuticals, Inc.) for the simultaneous induction of melanocytes, neurons and glia. Cultures were fed every third day by replacing the medium with 2 ml of fresh medium. After the cells had been cultured for 14 days, they were stained

with LacZ to confirm the presence of NC-derived cells and with specific antibodies to identify the types of colonies. For detection of LacZ activity, the cells were fixed in PBS solution (pH 7.4) containing 0.25% glutaraldehyde. After having been washed, they were stained with a solution containing Bluo-Gal (GIBCO-BRL) in N,N'-dimethylformamide for 8 h.

Antibodies and immunohistochemistry

On serial days after induction of the differentiation of thymic cells, the cultured cells were stained separately with the polyclonal rabbit anti-mouse dopachrome tautomerase (Dct) antibody (provided by V. Hearing; Laboratory of Cell Biology, National Institutes of Health, Bethesda, MD, USA; 33) or with the following mAbs: rat anti-mouse nerve growth factor receptor p75 (p75) (AB-N02; ATSBIO, Inc.), mouse anti-mouse β-tubulin III (TUJ1; Babco), mouse anti-porcine glial fibrillary acidic protein (GFAP) (GA-5; Neomarker, Inc.), rat anti-mouse erythroid lineage cells (TER119; PharMingen) or mouse anti-human HLA-DQ (Neomarker, Inc.). The cultured cells were fixed with 2% PFA. After a washing, the endogenous peroxidase activity was blocked with 0.3% hydrogen peroxide, and the cells were then incubated with the first antibody. The bound antibody was visualized by subsequent incubation with biotin-conjugated goat antibodies against mouse, rat or rabbit IgG followed by streptavidin–HRP (HistoMark™ Streptavidin–HRP Kit). After having been washed, the cells bearing immunocomplexes were visualized by using a Diaminobenzidine Reagent Set (Kirkegaard and Perry Laboratories, Inc.).

Statistical analysis

Data were presented as mean ± SD. Statistical significance was assessed by using Student's t-test.

Results

Tracing NC-derived cells in the fetal thymus by using the P0-Cre/Rosa26R mouse system

To assess the presence of NC-derived cells in the thymus, we constructed mice carrying the Cre gene under the control of the P0 promoter (P0-Cre), which expresses the Cre gene in the NC cell lineage (19). Crossing P0-Cre mice and Rosa26R mice, which carry LoxP-LacZ sequences, enabled us to trace NC-derived cells that had expressed the P0 gene as LacZ-expressing cells. LacZ⁺ cells were detected in organs including the mandible and heart, in which NC-derived cells were previously reported to be present, and in the thymus of E14.5 P0-Cre/Rosa26R double-transgenic (Tg) embryos (Fig. 1B). However, no LacZ⁺ cells were detected in age-matched Rosa26R embryos that did not carry P0-Cre Tg (Fig. 1A).

Temporal differences in the presence of NC-derived cells in the thymus

To clarify the spatial and temporal presence of NC-derived cells in the developing thymus, we stained P0-Cre/Rosa26R mice or Rosa26R mice from E11.5 to E18.5 for LacZ. As shown in Fig. 2, large numbers of LacZ⁺ (NC-derived) cells were detected in E11.5, E12.5, E14.5, E15.5 and E16.5 thymi, but these cells were rarely detected in the thymus beyond E17.5 in
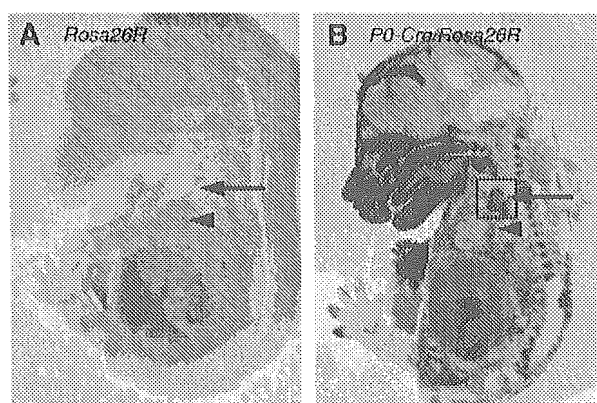

Fig. 1. Presence of NC-derived cells in the fetal thymus. Cells that expressed the P0 gene were detected by staining of E14.5 P0-Cre/Rosa26R double-Tg mice for LacZ (B). LacZ⁺ cells were present in the thymus (arrow) as well as in the face and heart (arrow head). No LacZ⁺ cells were present in any tissues of age-matched Rosa26R-Tg mice (A).

P0-Cre/Rosa26R embryos. As NC-derived cells were still detected in the heart and craniofacial region of E18.5 P0-Cre/Rosa26R embryos, the present duration of NC-derived cells in the thymus might be distinct from that in other organs (Fig. 2B).

To confirm the results obtained by LacZ staining, we performed flow cytometric analysis using FDG, which allows LacZ⁺ cells to be detected as living cells. Approximately 15% of the total thymic cells on E14.5, but only 2% on E18.5, were LacZ⁺ cells (Fig. 3A). These results agree with the data on whole-mount embryos stained for LacZ and suggest that the number of NC-derived cells decreased in the developing thymus as it became older. Furthermore, we could rarely detect NC-derived cells in the post-natal thymus (data not shown).

Spatial distribution of NC-derived cells in the thymus

To assess the distribution of NC-derived cells in the thymus, we prepared E14.5 and E18.5 thymic sections and stained them with hematoxylin and eosin and for LacZ. In E14.5 sections, the fetal thymus was surrounded by LacZ⁺ NC-derived cells (Fig. 3B). The region containing LacZ⁺ cells corresponded to that of mesenchymal cells surrounding the thymus. However, only a few NC-derived cells were present in the E18.5 thymus, and their location was restricted to marginal sites close to the heart (Fig. 2B').

One-third (32%) of E13.5 total thymic cells were NC-derived ones (Fig. 3C, left graph). To assess the distribution of NC-derived cells at the marginal sites of the thymus, we treated E13.5 thymi with Dispase II to divide them into the mesenchymal and epithelial regions. It is known that digestion with Dispase II keep the basement membrane intact. Single-cell suspensions were then prepared from each region, and flow cytometric analysis was performed on them. When we used cells from the mesenchymal region surrounding the thymus, nearly half of the cells expressed LacZ. In contrast, the proportion of NC-derived cells was decreased in the population from the epithelial region (Fig. 3C). These results suggest
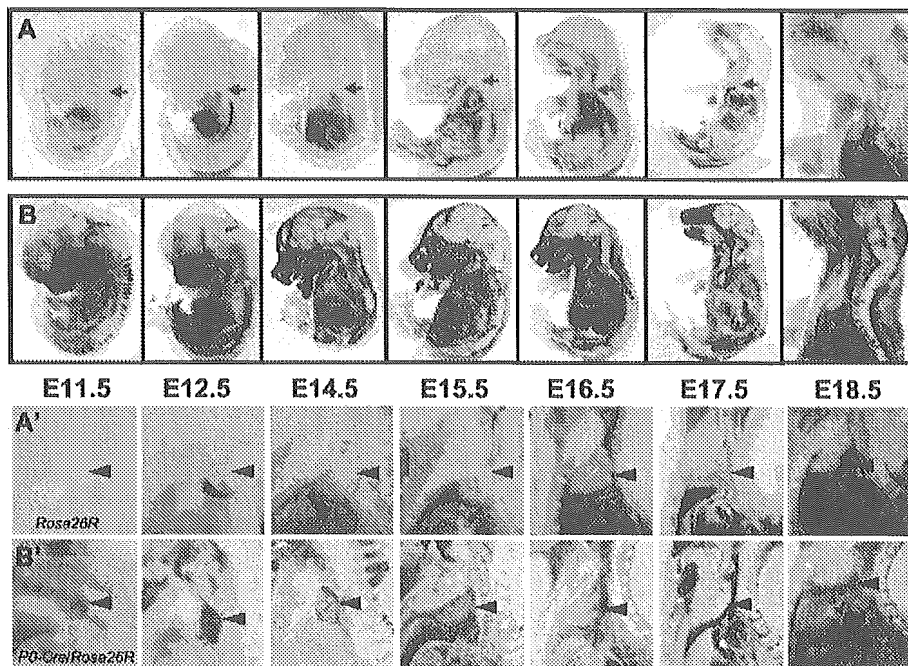
Fig. 2. Presence of NC-derived cells in the fetal thymus from E11.5 to E18.5. The thymi of E11.5 to E18.5 *Rosa26R-Tg* [A, A′(magnified)] and *P0-Cre/Rosa26R* double-Tg [B, B′(magnified)] mice were stained for LacZ (red arrows). Large numbers of LacZ⁺ NC-derived cells were detected in the *P0-Cre/Rosa26R* double-*Tg* thymus; however, their number was reduced beyond E17.5. The arrows in (A) and (B) and the arrowheads in (A′) and (B′) point to the thymus.

that a majority of the NC-derived cells were distributed in the mesenchyme surrounding the thymus, although a few of them had invaded the thymic epithelium.

Characterization of NC-derived cells in the fetal thymus

To characterize NC-derived cells in the thymus, we examined the expression of adhesion molecules on NC-derived cells of *P0-Cre/Rosa26R* mice using flow cytometric analysis. First, we examined the expression of CD45 on E13.5 mesenchymal cells surrounding thymi. LacZ⁺ cells rarely express CD45, indicating that NC do not contribute to hematopoietic cells in the thymus (data not shown). A majority of LacZ⁺ cells in the E13.5 mesenchymal cells surrounding thymi express integrin α5, αV, β1 and β3, and half of the LacZ⁺ cells express integrin α4 (Fig. 3D). However, larger numbers of LacZ-negative cells also express these molecules on the cell surface (Fig. 3D). It is known that mesenchymal cells are derived from both NC cells and mesodermal cells. These results may suggest that it is difficult to distinguish NC-derived mesenchymal cells from mesoderm-derived mesenchymal cells by the expression of adhesion molecules such as integrin family.

Presence of cells with the potential to differentiate into the melanocyte lineage in the fetal thymus

It is thought that melanocyte precursors might be distinct from neuronal and glial cell precursors or lose their potential to differentiate toward neuron or glial cell lineages before or soon

after the initiation of NC cell migration (24, 26). In fact, mature pigmented melanocytes are not normally present in the thymus. If NC-derived cells in the thymus give rise to melanocytes, they may be multipotent cells before committing to the melanocyte lineage. Therefore, to assess the potential of NC-derived cells in the murine thymus, we first investigated whether these cells could differentiate into melanocytes. Cells from C57BL/6 wild-type fetal and neonatal thymi were cultured on ST2 stromal cells with ET3 and DEX for 3 weeks (34). Pigmented melanocytes could be induced from E12.5, E14.5 and E15.5, but not from E18.5 or 3.5-day-old thymi (Table 1, Fig. 4A). In cultures of E14.5 thymic cells, the number of melanocytes was significantly decreased in the presence of BQ788, an antagonist of ETR-B (Fig. 4A).

Subsequently, using thymic cells from *P0-Cre/Rosa26R* double-*Tg* mice or *Rosa26R* mice, we performed melanocyte induction by using the same experimental protocol. Large numbers of colonies in the cultures from *P0-Cre/Rosa26R* double-*Tg* mice consisted of LacZ⁺ cells, and the majority of the cells with melanin granules expressed LacZ (Fig. 4C), whereas the *Rosa26R* cultures contained pigmented cells, but none was LacZ⁻ (Fig. 4B). Therefore, almost all cells that differentiated into melanocytes had expressed the *P0-Cre* gene. The frequency of LacZ⁺ cells forming colonies with pigmented melanocytes was ~1 per 10⁴ thymic cells (Table 3). Thus, a small but significant number of NC-derived cells in the fetal thymus were able to differentiate into melanocytes. The period when LacZ⁺ cells were present in the fetal thymus was
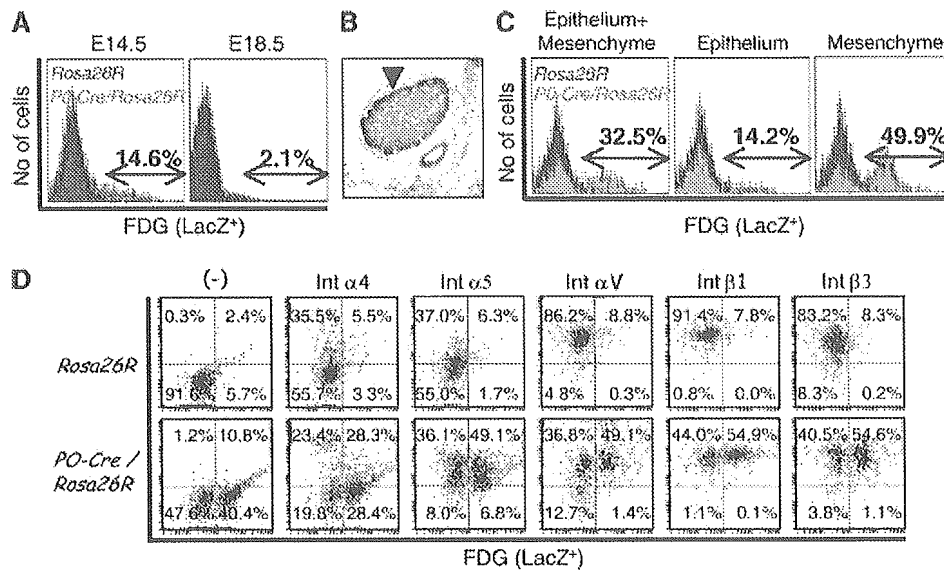
Fig. 3. Flow cytometric analysis of NC-derived cells in the thymus using FDG. (A) Cells from E14.5 or E18.5 thymi of *P0-Cre/Rosa26R* mice or *Rosa26R* mice were dissociated, and flow cytometric analysis was performed on the dissociated cells. Sections of E14.5 (B) and E18.5 (data not shown) thymi of *P0-Cre/Rosa26R* double-*Tg* mouse were stained for LacZ and also stained with hematoxylin and eosin. LacZ⁺ cells were present in the area surrounding the thymus (B: arrowhead). No LacZ⁺ cells were observed in the thymi of *Rosa26R* mice (data not shown). Next, E13.5 thymi were divided into mesenchyme and epithelium by treatment with Dispase II. (C) Cells from mesenchyme, epithelium and both were dissociated into single cells, and flow cytometric analysis was then performed on them. (D) The expression of adhesion molecules such as α4, α5, αV, β1 and β3 integrins on the mesenchymal cells surrounding thymi of E13.5 *P0-Cre/Rosa26R* mice. First, cells were stained with FDG to detect NC-derived cells, and then stained with antibodies against integrins.

mostly consistent with that when melanocyte precursors were present (Table 1). These results further confirm that LacZ⁺ cells in the thymus of *P0-Cre/Rosa26R* mice are derived from NCs.

Next, to detect immature melanocyte lineage cells, we stained cultured cells with an antibody directed against Dct, which is specifically expressed on melanocyte precursors or 'melanoblasts' (33). Both Dct⁺ melanoblasts and pigmented melanocytes were induced in the presence of ET3 and DEX (Fig. 4G), but neither of these types of cells was induced with DEX only (Fig. 4D and E). As neither Dct⁺ cell (data not shown) nor pigmented melanocyte was detected in the E14.5 thymus, NC-derived cells prior to expressing the *Dct* gene might be stimulated by mainly ET3–ETR-B signaling to give rise to Dct⁺ melanoblasts and pigmented melanocytes.

Presence of NC-derived cells in the fetal thymus with the potential to differentiate into multi-lineage cells

To determine whether NC-derived cells with the potential to differentiate into lineages other than the melanocyte lineage were present in the fetal thymus, we performed *in vitro* colony assays in the presence of ET3 with or without heregulin and forskolin, which strongly direct the differentiation of NC cells toward the glial cell lineage (35). Single cells from C57BL/6 thymi proliferated and formed a colony on day 14 of culture. The colonies from E14.5 or E15.5 thymic cells were characterized by the expression of p75 (a neuron and/or glial marker), β-tubulin III (a neuron-specific marker) or GFAP (a glia-specific marker) (Fig. 5). In some experiments, colonies were stained with a mixture of three antibodies against p75, β-tubulin III and

Table 1. Induction of melanocytes from fetal and post-natal C57BL/6 thymi in culture

	No. of melanocyte-containing cultures/No. of cultures examined				
Cells from	E12.5	E14.5	E15.5	E18.5	D3.5
+/+	2/5ᵃ	2/4ᵃ	4/8	0/6	0/6

Two hundred thousand cells from fetal to 3.5-day-old (D3.5) thymi of C57BL/6 (+/+) mice were cultured with ST2 cells in the presence of ET3 and DEX. After 3 weeks, pigmented melanocytes were observed under a light microscope.
ᵃSeveral thymic lobes were mixed and cultured in the case of E12.5 and E14.5 embryos to obtain 2 × 10⁵ thymic cells, while only a pair of thymic lobes were cultured in the case of embryos from E15.5 or thereafter. Similar results were obtained in another independent experiment.

GFAP (Fig. 5G and H). Colonies lacking both pigmented melanocytes and cells stained with antibodies directed against neurons and/or glias were omitted from the counting.

We identified three types of colonies: (i) pigmented melanocytes with melanin granules but no cells expressing neuronal or glial cell markers (named melanocyte colonies, Fig. 5A), (ii) p75⁺ (Fig. 5B), β-tubulin III⁺ or GFAP⁺ cells (data not shown) but no melanocytes (neuron and/or glial colonies) and (iii) melanocytes and p75⁺ (Fig. 5C), β-tubulin III⁺ (Fig. 5D) or GFAP⁺ cells (Fig. 5E) or cells stained by any three of the antibodies (Fig. 5H) (mixed colonies). As shown in Table 2, 4.5% (1 of 23 total colonies generated) of the colonies from
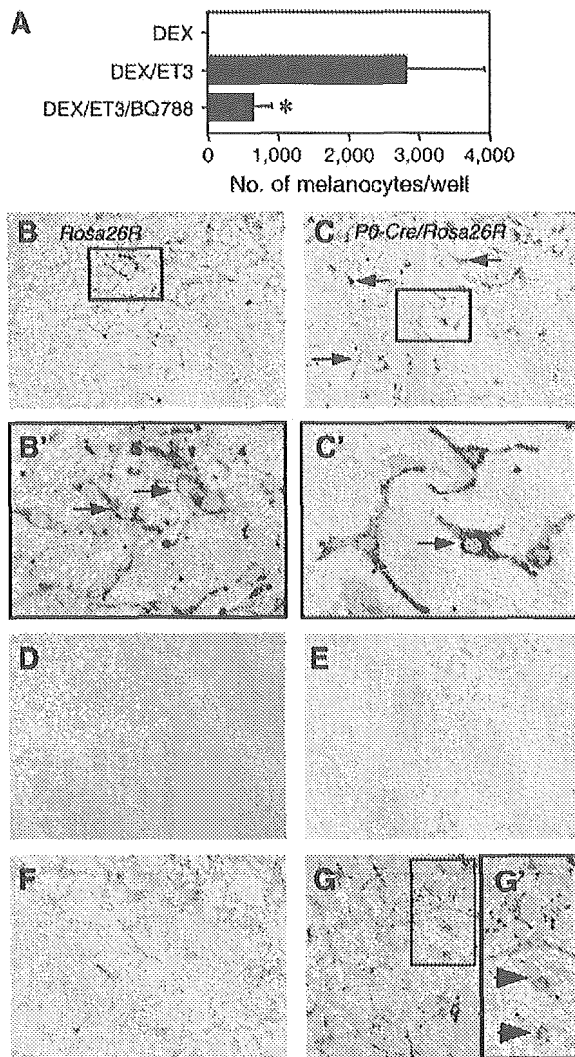
A

DEX

DEX/ET3

DEX/ET3/BQ788

0   1,000 2,000 3,000 4,000
No. of melanocytes/well

Fig. 4. Presence of cells with the potential to differentiate into melanocytes in the E14.5 thymus. (A) C57BL/6 E14.5 fetal thymic cells (2 × 10^5 per well) were cultured on ST2 stromal cells with DEX, DEX plus ET3 or DEX plus ET3 plus BQ788 for 3 weeks. The number of pigmented melanocytes (black cells) was then counted. Data are expressed as the mean ± SD of triplicate cultures. Asterisk indicates those significantly different from cultures with DEX + ET3 ($P < 0.05$). Next, E14.5 thymic cells from *P0-Cre/Rosa26R* double-*Tg* (C) and *Rosa26R-Tg* (B) mice were cultured in the presence of ET3. After 14 days, the cultured cells were stained for LacZ. The *P0-Cre/Rosa26R-Tg* cultures contained cells that were both pigmented (black) and LacZ⁻ (blue) [C, C'(magnified); arrows], whereas the *Rosa26R* cultures contained pigmented cells, but none was LacZ⁺ [B, B'(magnified); arrows]. Cultured cells treated with DEX (D, E) or with DEX + ET3 (F, G) were stained with rabbit anti-Dct antibody [E, G, G'(higher magnification)] to detect melanocyte precursors (melanoblasts: arrows) or with rabbit serum (D, F) as a control.

fetal thymi were p75⁺ neuronal and/or glial colonies without melanocytes (Fig. 5B). Approximately 79% of the colonies from thymic cells (18/23) were melanocyte colonies, and 16% (4/23) were mixed colonies (Table 2). The formation of these mixed colonies of either melanocytes and neurons or melanocytes

and glial cells thus indicate the presence of multipotent NC-derived cells (5, 36–38).

Using *P0-Cre/Rosa26R* double-*Tg* mice, we confirmed that the mixed colony-forming cells were NC-derived cells that expressed the *P0* gene (Fig. 5H). In a single colony (Fig. 5F), LacZ⁺ cells with melanin granules (arrows in Fig. 5H) and cells stained by the mixture of antibodies directed against neurons and/or glias (arrowhead in Fig. 5H) co-existed. Pigmented melanocytes did not express p75, β-tubulin III or GFAP (Fig. 5C–E and H). These results indicate that multipotent NC-derived cells were present in the fetal thymus. In this culture, half of the colonies were melanocyte colonies, as was the case for cultures from wild-type mice, 15% of them were mixed colonies containing both p75/β-tubulin/GFAP⁺ and pigmented cells and 30% of the colonies were neuronal and/or glial colonies containing p75/β-tubulin/GFAP⁺ (Table 3).

### NC-derived colony-forming cells were rarely detected in the E17.5 thymus

We showed that multipotent NC-derived cells were present in the E14.5 and E15.5 thymi (Fig. 5). When we assessed whether multipotent NC-derived cells were present in the thymus at late embryonic stages, few colonies were detected in cultures from the E17.5 thymus (Fig. 5I), confirming the rarity of NC-derived cells in the thymus after E17.5, as shown from the analysis of the *P0-Cre/Rosa26R* mice (Fig. 2).

Discussion

In this study, we showed that *P0-Cre/Rosa26R* mice were useful to trace NC-derived cells not only *in vivo* but also *in vitro*. Using these systems, we showed that NC-derived cells were mainly present in the area surrounding the thymus during E11.5 to E16.5 but were decreased in number beyond E17.5 and that NC-derived cells with the potential to differentiate into melanocyte, neuron and glia cell lineages were detected only during this same period.

Tracing NC-derived cells by using P0 promoter sequences

There is no specific marker for murine NC cells, unlike the case of HNK-1 for chickens and rats (39). Therefore, the promoters of *Pax3*, *Conexin43* and *Wnt1* genes have been used to detect the cranial NC cells containing cardiac NC cells (13, 40, 41). *Pax3-LacZ* and *Conexin43-LacZ* mice have provided the most reliable markers for the study of cardiac NC cell fate. Using mice bearing these markers, Waldo *et al.* detected NC cells in the E14 heart and thymus, but the expression of these transgenes was extinguished in mid- to late gestation (40). To trace the presence of NC-derived cells, we employed the promoter sequence of the *P0* gene, which promotes expression in migrating NC cells. The *P0* promoter sequence-driven *Cre* system as well as the human plasminogen activator–*Cre* system is useful for detecting not only cranial but also trunk NC-derived cells (19–21, 42), whereas the *Wnt1* promoter system allows the tracing of cranial NC cells only (13). We detected a large number of LacZ⁺ cells in the E12.5 to E15.5 thymi of *P0-Cre/Rosa26R* mice, whereas the number was significantly decreased in E17.5 thymi and thereafter. Flow cytometric analysis confirmed the presence of LacZ⁺ cells
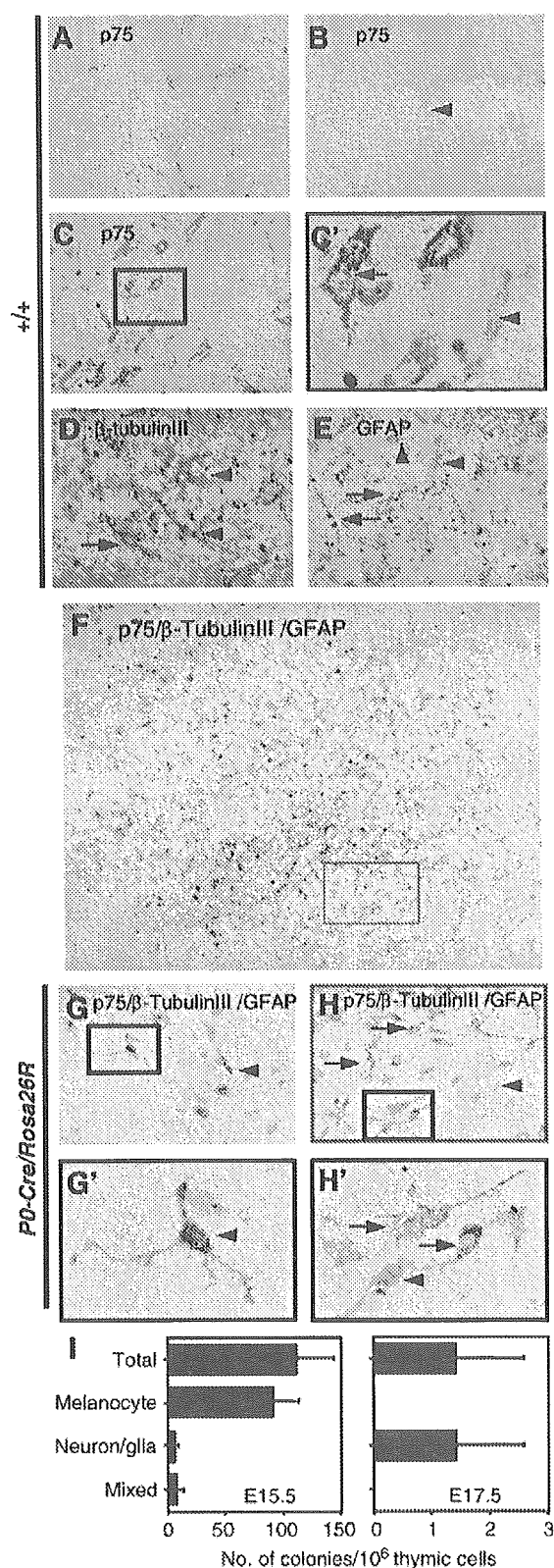
(~15%) in the E14.5 thymus and showed a significant reduction in their number (to ~2%) in the E18.5 thymus (Fig. 3). This finding is not unique to *P0-Cre/Rosa26R* mice, because similar observations were made when *Wnt1-Cre/Rosa26R* mice were examined (13). These results indicate that NC-derived cells contribute to thymic organogenesis and might explain why no melanocytes were induced in the E18.5 thymi of wild-type embryos (Table 1). However, a few NC-derived cells were still present in the E18.5 thymus; thus, it remains possible that they might have lost their potential to differentiate into melanocytes.

Presence of multipotent NC-derived cells in the fetal thymus

The melanocyte lineage has been thought to be derived only from the migrating NC cells through dorsolateral pathways (43). In contrast, posterior rhombencephalic NC cells that have migrated into posterior visceral arches have the potential to differentiate into neuronal cells, but not into melanocytes (3). Therefore, the commitment to the melanocyte lineage might occur in an early differentiation phase (3, 23, 24, 27). However, it is also reported that NC cells consist of heterogenous populations with the potential for differentiation (3, 4, 27). Therefore, there still remains the possibility that NC-derived cells in the developing thymus have a potential to differentiate only into melanocytes and neurons, or melanocytes and glial cells rather than multipotent NC-derived cells.

Recently, the presence of 'NC stem cells' that differentiate into glial cells, neurons and myofibroblasts in the sciatic nerve and gut of fetal rats was reported (5, 44). These stem cells were identified based on their expression of p75 molecules but not on that of other lineage markers for glial cells, neurons or myofibroblasts. However, these studies did not demonstrate the potential of these stem cells to differentiate into melanocytes. The culture conditions might not have permitted melanogenesis, or, alternatively, the stem cells isolated might have lacked melanogenic potential. In our culture system, we could not detect multipotent NC-derived cells with the potential to differentiate into myofibroblasts in the thymus. Our culture conditions might not have permitted such differentiation.

Fig. 5. Presence of multipotent NC-derived cells able to differentiate into melanocytes, neuronal and/or glial precursors in the fetal thymus. Colony formation by E15.5 (A–E) or E14.5 (F–H) fetal thymic cells was induced by culturing the cells on ST2 for 14 days in the presence of ET3, DEX, heregulin and forskolin. Colonies were stained with anti-p75 (A–C), anti-β-tubulin III (D), anti-GFAP (E) or a mixture of anti-p75, anti-β-tubulin III and anti-GFAP antibodies (F–H). Cells reactive with each antibody are stained brown (arrowheads), and black-pigmented cells (arrows) are melanocytes. (F) An NC-derived mixed colony with both melanocytes and neurons and/or glia cells. Colonies lacking both pigmented melanocytes and cells stained by antibodies directed against neurons and/or glia were omitted from the counting. NC-derived cells were detected as LacZ+ cells that had expressed *P0-Cre Tg* by using *P0-Cre/Rosa26R-Tg* mice (F–H). Higher magnifications of the boxed regions in (G) and (H) are shown in (G') and (H'), respectively. Rat and mouse mAbs against irrelevant molecules were used as controls, and no positive cells were observed in the colonies (data not shown, see Methods). Two hundred thousand cells from E15.5 or E17.5 (I) fetal thymi from C57BL/6 (+/+) mice were cultured and stained as described. 'Mixed colonies' contained both melanocytes and p75+ cells. This graph shows the number of colonies per 10^6 cells. Similar results were obtained in another independent experiment.

Table 2. Detection of melanocytes, neurons and/or glias in the colonies from fetal thymic cells

Colony type	No. of colonies/2 × 10^5 thymic cells
	+/+
Total colonies	22.7 ± 6.7 (100%)
Melanocyte colonies	18.0 ± 4.4 (79%)
Neuronal and/or glial colonies	1.0 ± 0.7 (4%)
Mixed colonies	3.7 ± 1.5 (16%)

Two hundred thousand cells from E15.5 fetal thymi from C57BL/6 (+/+) mice were cultured on ST2 in the presence of ET3, DEX, heregulin and forskolin. After 14 days, the cells were stained with anti-p75 mAb to identify the type of colonies (see caption of Fig. 5). A 'mixed colony' means that the colony contained both melanocytes and p75$^+$ cells. Similar results were obtained in another independent experiment.

Table 3. Detection of melanocytes, neurons and/or glias in the colonies from *P0-Cre/Rosa26R* E14.5 thymic cells

Colony type	No. of LacZ$^+$colonies/1 × 10^5 thymic cells
Total colonies	11.1 ± 5.3 (100%)
Melanocyte colonies	5.6 ± 2.7 (50%)
Neuronal and/or glial colonies	3.4 ± 1.4 (31%)
Mixed colonies	1.7 ± 1.9 (15%)
Others	0.4 ± 0.8 (4%)

One hundred thousand cells from E14.5 fetal thymi from *P0-Cre/Rosa26R* mice were cultured on ST2 in the presence of ET3, DEX, heregulin and forskolin. After 14 days, the cells were stained with a mixture of mAbs against p75/β-tubulin III/GFAP to identify the type of colonies (see caption of Fig. 5). A 'mixed colony' means that the colony contained both melanocytes and p75/β-tubulin III/GFAP$^+$ cells. The designation 'others' means LacZ$^-$ colonies melanocytes or p75/β-tubulin III/GFAP$^+$ cells. Similar results were obtained in another independent experiment.

Although large numbers of NC-derived cells were present in the thymus, they were rarely stained by specific antibodies directed against neurons, glias or melanocytes (data not shown). The majority of cells that expressed *P0* may have differentiated into cells of other lineages, or may have remained multipotent. The absence of melanocytes, neurons and glias in the normal thymus may result from the lack of proper microenvironmental factors for differentiation into these lineages. Here, we assessed only three cell lineages, namely melanocytes, neurons and glias. Analysis of additional cell lineages may reveal the precise roles of NC-derived cells in the thymus.

NC-derived cells and thymic organogenesis

The thymus is composed of both mesenchymal and epithelial cell components (6, 15). The thymic epithelium and mesenchyme are thought to be derived from the endoderm and/or ectoderm, and the mesoderm and/or NC cells, respectively (45–47). Thymic organogenesis is divided temporally into three stages, i.e. early (E9.5–E11), middle (E11.5–E15) and late (E15.5 to birth) (48). The early-stage-initiating thymic organogenesis is thought to be regulated by interactions between epithelial and mesenchymal cells (49–51).

In the middle stage, the patterning and initial epithelial differentiation occur in thymic rudiments, and T lymphocyte progenitors immigrate there (52–54). NC-derived cells are known to contribute to blood vessel formation, and they differentiate into pericytes surrounding vascular endothelial cells derived from the mesoderm (4, 55). Although in the middle stage, blood vessels have not yet formed in the thymus, mesenchymal cells surrounding the fetal thymus express the adhesion molecules that control migration and homing of hematopoietic cells. NC-derived cells are already present in the E11.5 thymus, meaning that cells of this lineage migrate into the thymus before hematopoietic cells. As shown in this study, NC-derived cells are mainly detected in the mesenchymal region surrounding the thymus, suggesting that NC-derived cells might help the immigration of T lymphocyte progenitors into the thymus (6, 8, 56).

Furthermore, we showed that integrin family members, such as integrin α4, α5, αV, β1 and β3 (Fig. 3), and CD44 (data not shown) were expressed on the cell surface of LacZ$^+$ cells (NC-derived cells) in the thymus. Previously, it was reported that signals via interaction between integrin receptors on mesenchyme and T progenitors are important for immigration of T progenitors into the thymus (57–59). These data suggest that NC-derived cells might play an important role in the immigration of T progenitor cells. Approximately 60% of the mesenchymal cells surrounding the E13.5 thymi express PDGFRα, and 70% in these PDGFRα$^+$ cells are LacZ$^+$ cells (derived from NC-derived cells) (H.Y., unpublished data). PDGFRα$^+$ cells are known to be important for thymic organogenesis because the mutation of this gene results in abnormalities of both the thymus and the heart (60, 61). As PDGFRα is expressed on both mesoderm-derived cells and NC-derived ones (62), it is not clear whether PDGFRα$^+$ NC-derived cells are important for thymic organogenesis (62).

NC-derived cells and the late stages of thymic organogenesis

In the late stage, thymic epithelial cells have acquired the functional competence for supporting T lymphocyte development. In this stage, NC-derived cells are rarely detected, and T progenitors immigrate into the thymus through blood vessels in the cortical–medullar junction (63), suggesting that NC-derived cells might not be required during this stage. It is thought that these blood vessels are derived from the mesoderm and not from NC-derived cells. Petrie proposed that NC-derived cells have a minor role in thymic organogenesis after birth because few NC-derived cells were observed in the *Wnt1-Cre/Rosa26R* thymus at that time (13, 64).

Le Douarin and Jotereau (8) reported that avian NC cells contribute to thymic connective tissues, which are especially located in interlobular sites in the cortex and lining blood vessels in the cortex and medulla of the gland (65). Considering these previous reports, thymic NC-derived cells might likely be considered to be detected in the thymic cortex and medulla of murine embryos at a late stage. However, in E17.5 and E18.5 *P0-Cre/Rosa26R* mice as well as in *Wnt1-Cre/Rosa26R* mice, only a few NC-derived cells were present, and their location was restricted to the epithelial marginal sites of the thymic lobes (Figs 2 and 3). However, the possibility

cannot be ruled out that these promoters might not label NC cells completely. Alternatively, NC-derived cells that do not express *P0* or *Wnt1* might contribute to the thymic organogenesis at late embryonic stages. The roles of NC-derived cells may not be identical in avian and murine systems.

Conclusions

In this study, to assess both spatially and temporally the presence and the potential of NC-derived cells in the thymus, we traced NC-derived cells and developed a colony formation assay system. It is likely that NC-derived cells in the thymus retain multipotency, but are only present during a restricted period of thymogenesis.

In the heart and craniofacial area, NC-derived cells are continuously present and contribute to the organogenesis from the embryonic stage to adult life (13). However, the fact that NC-derived cells are only present in the thymus of early embryos may indicate the existence of an as yet unknown system that contributes to the organogenesis. Further studies using our system will yield important information on the role of NC-derived cells in thymic organogenesis.

Acknowledgements

Abbreviations

Dct	dopachrome tautomerase
DEX	dexamethasone
E	embryonic day
ET3	endothelin 3
ETR-B	endothelin receptor B
FBS	fetal bovine serum
FDG	fluorescein di-β-D-galactopyranoside
GFAP	glial fibrillary acidic protein
HNK	Human natural killer
NC	neural crest
P0	myelin protein zero
p75	nerve growth factor receptor p75
Tg	transgenic

References

1 Anderson, D. J. 1997. Cellular and molecular biology of neural crest cell lineage determination. *Trends Genet.* 13:276.

2 Bronner-Fraser, M. 1995. Origin and developmental potential of the neural crest. *Exp. Cell Res.* 218:405.

3 Ito, K. and Sieber-Blum, M. 1993. Pluripotent and developmentally restricted neural-crest-derived cells in posterior visceral arches. *Dev. Biol.* 156:191.

4 Le Douarin, N. M. and Kalcheim, C. 1999. Cell lineage segregation during neural crest ontogeny. In Le Douarin. N. M. and Kalcheim, C., eds., *The Neural Crest*, p. 304. Cambridge University Press, Cambridge.

5 Morrison, S. J., White, P. M., Zock, C. and Anderson, D. J. 1999. Prospective identification. isolation by flow cytometry, and *in vivo* self-renewal of multipotent mammalian neural crest stem cells. *Cell* 96:737.

6 Anderson, G. and Jenkinson, E. J. 2001. Lymphostromal interactions in thymic development and function. *Nat. Rev. Immunol.* 1:30.

7 Bockman. D. E. and Kirby, M. L. 1984. Dependence of thymus development on derivatives of the neural crest. *Science* 223:498.

8 Le Douarin, N. M. and Jotereau, F. V. 1975. Tracing of cells of the avian thymus through embryonic life in interspecific chimeras. *J. Exp. Med.* 142:17.

9 Manley, N. R. and Blackburn, C. C. 2003. A developmental look at thymus organogenesis: where do the non-hematopoietic cells in the thymus come from? *Curr. Opin. Immunol.* 15:225.

10 Merscher, S., Funke, B., Epstein, J. A. *et al.* 2001. TBX1 is responsible for cardiovascular defects in velo-cardio-facial/DiGeorge syndrome. *Cell* 104:619.

11 Epstein, J. A., Li, J., Lang, D. *et al.* 2000. Migration of cardiac neural crest cells in Splotch embryos. *Development* 127:1869.

12 Vitelli, F., Morishima, M., Taddei, I., Lindsay, E. A. and Baldini, A. 2002. Tbx1 mutation causes multiple cardiovascular defects and disrupts neural crest and cranial nerve migratory pathways. *Hum. Mol. Genet.* 11:915.

13 Jiang. X., Rowitch, D. H., Soriano, P., McMahon, A. P. and Sucov, H. M. 2000. Fate of the mammalian cardiac neural crest. *Development* 127:1607.

14 Anderson, G., Moore, N. C., Owen, J. J. and Jenkinson, E. J. 1996. Cellular interactions in thymocyte development. *Annu. Rev. Immunol.* 14:73.

15 Blackburn, C. C. and Manley, N. R. 2004. Developing a new paradigm for thymus organogenesis. *Nat. Rev. Immunol.* 4:278.

16 Kuratani, S. and Bockman, D. E. 1990. Impaired development of the thymic primordium after neural crest ablation. *Anat. Rec.* 228:185.

17 Kuratani, S. and Bockman, D. E. 1990. The participation of neural crest derived mesenchymal cells in development of the epithelial primordium of the thymus. *Arch. Histol. Cytol.* 53:267.

18 Soriano, P. 1999. Generalized lacZ expression with the Rosa26 Cre reporter strain. *Nat. Genet.* 21:70.

19 Yamauchi, Y., Abe, K., Mantani, A. *et al.* 1999. A novel transgenic technique that allows specific marking of the neural crest cell lineage in mice. *Dev. Biol.* 212:191.

20 Yamazaki, H., Yoshino, M. and Hayashi, S. 2005. Neural crest stem cells and organogenesis. In F. Columbus., ed. In *Progress in Stem Cell Research*. Nova Science Publisher Inc. NY, in press.

21 Yamazaki, H., Kurino, T., Sakata, E., Yoshino, M. and Hayashi, S.-I. 2003. Tooth development and tooth regeneration using tooth germ, dental pulp cells, neural crest cells and embryonic stem cells. *Recent Res. Develop. Biophys. Biochem.* 3:907.

22 Baroffio, A., Dupin, E. and Le Douarin. N. M. 1991. Common precursors for neural and mesectodermal derivatives in the cephalic neural crest. *Development* 112:301.

23 Erickson, C. A. and Goins, T. L. 1995. Avian neural crest cells can migrate in the dorsolateral path only if they are specified as melanocytes. *Development* 121:915.

24 Luo. R., Gao, J., Wehrle-Haller, B. and Henion, P. D. 2003. Molecular identification of distinct neurogenic and melanogenic neural crest sublineages. *Development* 130.321.

25 Noden, D. M. 1988. Interactions and fates of avian craniofacial mesenchyme. *Development* 103(Suppl.):121.

26 White, P. M. and Anderson, D. J. 1999. *In vivo* transplantation of mammalian neural crest cells into chick hosts reveals a new autonomic sublineage restriction. *Development* 126:4351.

27 Henion, P. D. and Weston, J. A. 1997. Timing and pattern of cell fate restrictions in the neural crest lineage. *Development* 124:4351.

28 Lahav. R., Dupin, E., Lecoin, L. *et al.* 1998. Endothelin 3 selectively promotes survival and proliferation of neural crest-derived glial and melanocytic precursors *in vitro. Proc. Natl Acad. Sci. USA* 95:15214.

29 Baynash, A. G.. Hosoda, K., Giaid, A. *et al.* 1994. Interaction of endothelin-3 with endothelin-B receptor is essential for development of epidermal melanocytes and enteric neurons. *Cell* 79:1277.

30 Yoshida. H., Kunisada, T., Kusakabe, M., Nishikawa, S. and Nishikawa, S.-I. 1996. Distinct stages of melanocyte differentiation

revealed by analysis of nonuniform pigmentation patterns. *Development* 122:1207.

31 Abe, K., Hashiyama, M., Macgregor, G. and Yamamura, K. 1996. Purification of primordial germ cells from TNAPbeta-geo mouse embryos using FACS-gal. *Dev. Biol.* 180.468.

32 Nishikawa, S., Ogawa, M., Nishikawa, S., Kunisada, T. and Kodama, H. 1988. B lymphopoiesis on stromal cell clone: stromal cell clones acting on different stages of B cell differentiation. *Eur. J. Immunol.* 18:1767.

33 Tsukamoto, K., Jackson, I. J., Urabe, K., Montague, P. M. and Hearing, V. J. 1992. A second tyrosinase-related protein, TRP-2, is a melanogenic enzyme termed DOPAchrome tautomerase. *EMBO J.* 11:519.

34 Yamane, T., Hayashi, S. I., Mizoguchi, M., Yamazaki, H. and Kunisada, T. 1999. Derivation of melanocytes from embryonic stem cells in culture. *Dev. Dyn.* 216:450.

35 Shah, N. M., Marchionni, M. A., Isaacs, I., Stroobant, P. and Anderson, D. J. 1994. Glial growth factor restricts mammalian neural crest stem cells to a glial fate. *Cell* 77:349.

36 Ito, K., Morita, T. and Sieber-Blum, M. 1993. *In vitro* clonal analysis of mouse neural crest development. *Dev. Biol.* 157:517.

37 Yamazaki, H., Kunisada, T., Yamane, T. and Hayashi, S. I. 2001. Presence of osteoclast precursors in colonies cloned in the presence of hematopoietic colony-stimulating factors. *Exp. Hematol.* 29:68.

38 Trentin, A., Glavieux-Pardanaud, C., Le Douarin, N. M. and Dupin, E. 2004. Self-renewal capacity is a widespread property of various types of neural crest precursor cells. *Proc. Natl Acad. Sci. USA* 101:4495.

39 Bronner-Fraser, M. 1986. Analysis of the early stages of trunk neural crest migration in avian embryos using monoclonal antibody HNK-1. *Dev. Biol.* 115: 44.

40 Waldo, K., Lo, C. W. and Kirby, M. L. 1999. Connexin 43 expression reflects neural crest patterns during cardiovascular development. *Dev. Biol.* 208:307.

41 Natoli, T. A., Ellsworth, M. K., Wu, C., Gross, K. W. and Pruitt, S. C. 1997. Positive and negative DNA sequence elements are required to establish the pattern of *Pax3* expression. *Development* 124:617.

42 Pietri, T., Eder, O., Blanche, M., Thiery, J. P. and Dufour, S. 2003. The human tissue plasminogen activator–Cre mouse: a new tool for targeting specifically neural crest cells and their derivatives *in vivo*. *Dev. Biol.* 259:176.

43 Mayer, T. C. 1973. The migratory pathway of neural crest cells into the skin of mouse embryos. *Dev. Biol.* 34:39.

44 Kruger, G. M., Mosher, J. T., Bixby, S., Joseph, N., Iwashita, T. and Morrison, S. J. 2002. Neural crest stem cells persist in the adult gut but undergo changes in self-renewal, neuronal subtype potential, and factor responsiveness. *Neuron* 35:657.

45 Cordier, A. C. and Heremans, J. F. 1975. Nude mouse embryo: ectodermal nature of the primordial thymic defect. *Scand. J. Immunol.* 4:193.

46 Bennett, A. R., Farley, A., Blair, N. F., Gordon, J., Sharp, L. and Blackburn, C. C. 2002. Identification and characterization of thymic epithelial progenitor cells. *Immunity* 16:803.

47 Gill, J., Malin, M., Hollander, G. A. and Boyd, R. 2002. Generation of a complete thymic microenvironment by MTS24(+) thymic epithelial cells. *Nat. Immunol.* 3:635.

48 Manley, N. R. 2000. Thymus organogenesis and molecular mechanisms of thymic epithelial cell differentiation. *Semin. Immunol.* 12:421.

49 Klug, D. B., Carter, C., Gimenez-Conti, I. B. and Richie, E. R. 2002. Cutting edge: thymocyte-independent and thymocyte-dependent phases of epithelial patterning in the fetal thymus. *J. Immunol.* 169:2842.

50 Jenkinson, W. E., Jenkinson, E. J. and Anderson, G. 2003. Differential requirement for mesenchyme in the proliferation and maturation of thymic epithelial progenitors. *J. Exp. Med.* 198:325.

51 Suniara, R. K., Jenkinson, E. J. and Owen, J. J. 2000. An essential role for thymic mesenchyme in early T cell development. *J. Exp. Med.* 191:1051.

52 Suniara, R. K., Jenkinson, E. J. and Owen, J. J. 1999. Studies on the phenotype of migrant thymic stem cells. *Eur. J. Immunol.* 29:75.

53 Wilkinson, B., Owen, J. J. and Jenkinson, E. J. 1999. Factors regulating stem cell recruitment to the fetal thymus. *J. Immunol.* 162:3873.

54 Itoi, M., Kawamoto, H., Katsura, Y. and Amagai, T. 2001. Two distinct steps of immigration of hematopoietic progenitors into the early thymus anlage. *Int. Immunol.* 13:12031.

55 Etchevers, H. C., Vincent, C., Le Douarin, N. M. and Couly, G. F. 2001. The cephalic neural crest provides pericytes and smooth muscle cells to all blood vessels of the face and forebrain. *Development* 128:1059.

56 Bockman, D. E. and Kirby, M. L. 1985. Neural crest interactions in the development of the immune system. *J. Immunol.* 135(Suppl.): 766.

57 Anderson, G., Anderson, K. L., Tchilian, E. Z., Owen, J. J. and Jenkinson, E. J. 1997. Fibroblast dependency during early thymocyte development maps to the CD25+ CD44+ stage and involves interactions with fibroblast matrix molecules. *Eur. J. Immunol.* 27:1200.

58 Salomon, D. R., Mojcik, C. F., Chang, A. C. *et al.* 1994. Constitutive activation of integrin alpha 4 beta 1 defines a unique stage of human thymocyte development. *J. Exp. Med.* 179:1573.

59 Godfrey, D. I., Kennedy, J., Suda, T. and Zlotnik, A. 1993. A developmental pathway involving four phenotypically and functionally distinct subsets of CD3–CD4–CD8– triple-negative adult mouse thymocytes defined by CD44 and CD25 expression. *J. Immunol.* 150:4244.

60 Soriano, P. 1997. The PDGF alpha receptor is required for neural crest cell development and for normal patterning of the somites. *Development* 124:2691.

61 Tallquist, M. D. and Soriano, P. 2003. Cell autonomous requirement for PDGFRalpha in populations of cranial and cardiac neural crest cells. *Development* 130:507.

62 Takakura, N., Yoshida, H., Ogura, Y., Kataoka, H., Nishikawa, S. and Nishikawa, S. 1997. PDGFR alpha expression during mouse embryogenesis: immunolocalization analyzed by whole-mount immunohistostaining using the monoclonal anti-mouse PDGFR alpha antibody APA5. *J. Histochem. Cytochem.* 45:883.

63 Petrie, H. T. 2003. Cell migration and the control of post-natal T-cell lymphopoiesis in the thymus. *Nat. Rev. Immunol.* 3:859.

64 Petrie, H. T. 2002. Role of thymic organ structure and stromal composition in steady-state postnatal T-cell production. *Immunol. Rev.* 189:8.

65 Le Douarin, N. M. 1978. Ontogeny of hematopoietic organs studied in avian embryo interspecific chimeras. In Clarkson, B., Marks, P. A. and Till, J. E., eds., *Differentiation of Normal and Neoplastic Hematopoietic Cells*, p. 5. Cold Spring Harbor Laboratory, Cold Spring Harbor, NY.

A Novel Murine Gene, *Sickle tail*, Linked to the *Danforth's short tail* Locus, Is Required for Normal Development of the Intervertebral Disc

Kei Semba,[*,†] Kimi Araki,[*] Zhengzhe Li,[*] Ken-ichirou Matsumoto,[*,†] Misao Suzuki,[‡]
Naoki Nakagata,[§] Katsumasa Takagi,[†] Motohiro Takeya,[**] Kumiko Yoshinobu,[††]
Masatake Araki,[††] Kenji Imai,[‡‡] Kuniya Abe[§§] and Ken-ichi Yamamura[*,1]

*Division of Developmental Genetics, Institute of Molecular Embryology and Genetics, Kumamoto University, Kumamoto 862-0976, Japan,
†Department of Orthopaedic Surgery, Kumamoto University School of Medicine, Kumamoto 860-8556, Japan, ‡Division of Transgenic
Technology, Institute of Resource Development and Analysis, Kumamoto University, Kumamoto 860-0811, Japan, §Division of
Reproductive Engineering, Institute of Resource Development and Analysis, Kumamoto University, Kumamoto 860-0811,
Japan, **Department of Cell Pathology, Kumamoto University School of Medicine, Kumamoto 860-8556, Japan,
††Division of Bioinformatics, Institute of Resource Development and Analysis, Kumamoto University,
Kumamoto 860-0811, Japan, ‡‡Institute of Developmental Genetics, GSF-National Research Center
for Environment and Health, 85764 Neuherberg, Germany and §§Technology
Development Team for Mammalian Cellular Dynamics, BioResource
Center, RIKEN, Tsukuba, Ibaraki 305-0074 Japan

ABSTRACT

We established the mutant mouse line, B6;CB-*Skt*[Gt(pGT0pfs)82limeG] (*Skt*[Gt]), through gene-trap mutagenesis in embryonic stem cells. The novel gene identified, called *Sickle tail* (*Skt*), is composed of 19 exons and encodes a protein of 1352 amino acids. Expression of a reporter gene was detected in the notochord during embryogenesis and in the nucleus pulposus of mice. Compression of some of the nuclei pulposi in the intervertebral discs (IVDs) appeared at embryonic day (E) 17.5, resulting in a kinky-tail phenotype showing defects in the nucleus pulposus and annulus fibrosus of IVDs in *Skt*[Gt/Gt] mice. These phenotypes were different from those in *Danforth's short tail* (*Sd*) mice in which the nucleus pulposus was totally absent and replaced by peripheral fibers similar to those seen in the annulus fibrosus in all IVDs. The *Skt* gene maps to the proximal part of mouse chromosome 2, near the *Sd* locus. The genetic distance between them was 0.95 cM. The number of vertebrae in both [*Sd* +/+ *Skt*[Gt]] and [*Sd Skt*[Gt]/+ +] compound heterozygotes was less than that of *Sd* heterozygotes. Furthermore, the enhancer trap locus *Etl4*[lacZ], which was previously reported to be an allele of *Sd*, was located in the third intron of the *Skt* gene.

THE notochord is an integral component of the axial structure of vertebrates, functions as a signaling center during embryogenesis, and plays essential roles in patterning of both somites and the neural tube (ANG and ROSSANT 1994; WILSON *et al.*1995; CHIANG *et al.*1996). In addition, the notochord has major roles in vertebral column formation. In the mouse, the notochord is a continuous rod of constant diameter extending from the hypophysis to almost the tip of the tail at embryonic day (E) 9.5. At E10.5–E11.5, signals from the notochord induce the migration, proliferation, and fusion of the sclerotome to form a continuous and unsegmented perichordal tube around the notochord and neural tube. At 12.5, mesenchyme acquires a char-

acteristic metameric pattern of densely packed areas caudally and loosely packed areas cranially. Some densely packed cells move cranially and give rise to the annulus fibrosus of the future intervertebral disc (IVD). The remaining densely packed cells fuse with the immediately caudal loosely packed cells to form the cartilaginous primordia of the vertebral bodies. Notochord cells located in the vertebral body of cranial regions start to relocate into intervertebral regions (PAAVOLA *et al.* 1980; RUFAI *et al.* 1995; ASZODI *et al.* 1998). At E13.5, the vertebral regions are enlarged and chondrified. The notochord proliferates and undergoes hypertrophy to form the gelatinous center of the intervertebral disc, called the nucleus pulposus. This nucleus is surrounded by the circularly arranged fibers of the annulus fibrosus. These two structures together constitute the IVD (LANGMAN 1969; THEILER 1988). At E14.5, nearly all chondrocytes are hypertrophied. Starting from E14.5, the annulus fibrosus can be subdivided into a fibrous outer annulus and a cartilaginous inner annulus. At E16.0, notochord cells complete relocation from vertebral regions into

intervertebral regions. Failures in somite, neural tube, and notochord formation are closely correlated with vertebral malformations. However, the mechanisms that underlie the formation of IVDs are largely unknown.

In the mouse, several mutations are known to affect the formation of the vertebral column due to functional defects in the notochord, including *Danforth's short tail* (*Sd*) and the enhancer trap line (*Etl4^{lacZ}*). *Sd*, located on chromosome 2 (LANE and BIRKENMEISER 1993; ALFRED *et al.* 1997), is a semidominant mutation affecting the development of the vertebral column and the urogenital system (DUNN *et al.* 1940; GRUNEBERG 1953, 1958). At E9.5, the notochord shows discontinuities. At E11.5, mesenchymal organization around the notochord is abnormal. At E13.5, the notochord is fragmented and does not show proliferation and dilatation. Chondrification is much reduced in vertebral regions. Thus, an early reduction of the notochord results in cellular degeneration in the sclerotome, leading to reduced vertebral bodies and a characteristic short tail due to a reduced number of caudal vertebrae. Homozygous *Sd* animals show a similar but much more severe tailless phenotype. In the enhancer trap line, *Etl4^{lacZ}*, a reporter (*lacZ*) gene was inserted near the *Sd* locus and was expressed in the notochord, mesonephric mesenchyme, and apical ectoderm ridge (GOSSLER *et al.* 1989; KORN *et al.* 1992; MAATMAN *et al.* 1997; ZACHGO *et al.* 1998). *Etl4^{lacZ}* homozygotes exhibited kinks in the caudal region of their tails and a synergistic genetic interaction between *Etl4^{lacZ}* and *Sd* was observed. Genetically, *Etl4^{lacZ}* and *Sd* are separated by 0.75 cM. Interestingly, attenuation or enhancement of the *Sd* phenotype was observed when the *Etl4^{lacZ}* insertion was in a *cis*- or *trans*-conformation, respectively. This suggests that *Etl4^{lacZ}* is an allele of *Sd*, presumably by trapping a *cis*-regulatory element of the *Sd* gene, and that *Sd* is a gain-of-function mutation (ZACHGO *et al.* 1998). Nevertheless, neither the *cis*-element nor the trapped gene has been identified.

In this study, we report a new mutant mouse line, *Skt^{Gt}*, obtained by gene-trap mutagenesis in embryonic stem (ES) cells. *Skt^{Gt/Gt}* mice exhibit a kinky tail in the caudal vertebral columns due to malformation of the IVDs. The gene identified, *Sickle tail* (*Skt*), was expressed in the notochord, its derivative nucleus pulposus, and in the mesonephros. Interestingly, the *Skt* gene maps to the proximal part of mouse chromosome 2, near the locus for *Sd*, and the *lacZ* insertion site in *Etl4^{lacZ}* was found to be located in the third intron of the *Skt* gene. Furthermore, a cumulative effect of the *Skt^{Gt}* mutation on the *Sd* mutant was observed.

MATERIALS AND METHODS

Generation and genotyping of mutant mice: The gene-trap method using the pU-8 trap vector was previously described (ARAKI *et al.* 1999). Chimeric mice were produced by the ag-

gregation method using ES gene-trap clones and morulas of ICR (Charles River, Wilmington, MA) mice, and the chimeric mice were mated with C57BL/6 (CLEA) females to obtain F_1 heterozygotes. *Sd* mice were purchased from the Jackson Laboratory (Bar Harbor, ME) and propagated by *in vitro* fertilization. *Sd* + / + × *Skt^{Gt}* mice were generated by mating *Sd* + / + + mice (C57BL/6 genetic background) to *Skt^{Gt/Gt}* mice with a C57BL/6 genetic background. One heterozygote carrying the *Sd* mutation and the *Skt^{Gt}* insertion on the same chromosome (*Sd Skt^{Gt}*/ + +; *cis*-configuration) was obtained through mating between *trans*-heterozygotes and wild-type C57BL/6 mice. *Sd* mice were distinguished by external inspection. Genotyping for *Skt^{Gt}* alleles was done with PCR using tail genomic DNA as a template. For the wild-type allele, the 5' primer, GT5 (5'-CCACCCCTACATGTGTCTTT-3'), and the 3' primer, GTA (5'-CGAGTAAGTAACATCCCTCC-3') located in the 14th intron, were used to generate a 339-bp wild-type fragment. To detect the trapped allele, the 5' primer, called Z1 (5'-GCGTT ACCCAACTTAATCG-3'), and the Z2 (5'-TGTGAGCGAGTAA CAACCCG-3') located in *lacZ* gene, were used to generate a 320-bp fragment.

Skeletal preparations: After tail skins were peeled off, tails were fixed in 95% ethanol for 3 days. Tails were cleared by placing in 1% KOH for 1 day and were stained in alizarin red for 1 day until the bone was red. Excess stain was removed with 2% KOH. After removing excessive alizarin red stain, tails were transferred to glycerol (HOGAN *et al.* 1994).

To count the number of vertebral bodies, we examined all mice by X-ray photography. We counted the number of normal vertebral bodies, that is, those without obvious malformations, but did not consider the size reduction observed in the vertebral bodies of *Sd* mutants.

Cloning of genomic DNA and cDNA: Plasmid rescue to obtain flanking genomic DNA was performed as described (ARAKI *et al.* 1999). The 5'-end of the cDNA of the trapped gene was isolated by 5'-rapid amplification of cDNA ends (5'-RACE) using the 5'-RACE system (Invitrogen, Carlsbad, CA). Total RNA from a B6;CB-*Skt^{Gt(pU8021)MEG}* gene-trapped ES clone was extracted by using Sepasol-RNA I (NACALAI TESQUE, Kyoto, Japan), and then poly(A)+ RNA was isolated with an oligo(dT) column (Takara Biomedicals, Shiga, Japan). First-strand cDNA synthesis from 1 μg of poly(A)+ RNA was performed with reverse transcriptase from ReverScript (Wako, Osaka, Japan) and with the primer SA13 (5'-TCTGAAACT CAGCCTTGAGC-3') in the splice acceptor (SA) sequence. After dCTP tailing with terminal deoxynucleotidyl transferase (Invitrogen), cDNA was purified using a QIAquick nucleotide removal kit (QIAGEN, Chatsworth, CA). The initial PCR was performed using the primer SA10 (5'-AGCAGTGAAGGCTGT GCGA-3') in the SA sequence and the anchor primer (5'-GGCCACGCGTCGACTAGTACGGGiiGGGiiGGGiiG-3') (Invitrogen). Then, nested PCR was performed using primer 63 (5'-GCTTGTCCTCTTTGTTAGGG-3') in the SA sequence and the amplification primer (5'-GGCCACGCGTCGACTAGTAC-3') in the anchor primer sequence. Amplified fragments were then sequenced directly by the dideoxy-chain termination method using Big Dye terminator cycle sequencing (Perkin-Elmer, Foster City, CA).

RT–PCR analysis: RT–PCR was performed using the Thermoscript RT–PCR system (Invitrogen) according to the manufacturer's instructions. The PCR was performed using the primers a–f in the sense and antisense sequences in the *Skt* gene. The sequences of the primers used are as follows: primer-a, 5'-TCACCATGAAGATGCTGGAG-3'; primer-b, 5'-CTACAG TAAGCACTCGCTGAC-3'; primer-c, 5'-ACTCCTCAGCGTTG ATGAAC-3'; primer-d, 5'-GTGGTGGTAAGTCCTGATCC-3'; primer-e, 5'-GCCACCTTAAAGACACTAGG-3'; and primer-f, 5'-TGAGGAGGAAGAGGTAGTAG-3'. The PCR conditions were
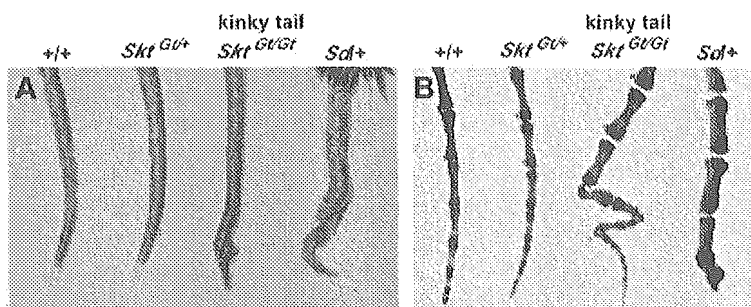
FIGURE 1.—(A) Tail phenotype of 8-week-old mice. *Skt^{Gt/Gt}* mice had kinked tails compared to wild-type, *Skt^{+/+}*, and heterozygous *Sd* mice. (B) Alizarin red whole-mount preparations of the tails of 8-week-old mice. *Skt^{Gt/Gt}* mice confirmed this kinky-tail phenotype. *Sd* mice showed decreased numbers of vertebrae with truncation at the caudal vertebrae.

94° for 1 min, 55° for 2 min, and 72° for 2 min using 0.5 units of Taq polymerase for 30 cycles.

Northern blot analysis: Total RNA and poly(A)+ mRNA isolated from ES cells and embryo and adult tissues were electrophoresed on a 0.7% denaturing formaldehyde-MOPS-containing agarose gel and transferred to a positively charged nylon membrane (Roche). After baking at 80° for 1 hr, the membrane was prehybridized and then hybridized using the *Skt* gene-specific RNA probes and the *lacZ* RNA probes prepared using DIG RNA labeling and detection kit (Roche).

Detection of β-galactosidase (lacZ) activities: Whole-mount X-gal staining was performed according to the method of ALLEN *et al.* (1988). Samples were fixed for 30 min at room temperature in fix solution [1% formaldehyde, 0.2% glutaraldehyde, and 0.02% NP-40 in phosphate-buffered saline (PBS)]. Fixed samples were washed two times in PBS and incubated overnight at 30° in staining solution (5 mM potassium ferricyanide, 5 mM potassium ferrocyanide, 2 mM MgCl₂, 0.5% X-gal in PBS). Samples were rinsed twice in PBS, postfixed in 4% paraformaldehyde, and made transparent using benzylalcohol/benzylbenzoate (1:2) after dehydration with a series of ethanol steps (25, 50, 70, 100, and 100%, 1 hr each). Adult tissues were fixed in 4% paraformaldehyde in PBS. Tissue sections of 10 μm were prepared and stained overnight at 30° with X-gal in staining solution. After staining, sections were counterstained with Fast Red. For the section of the intervertebral discs, after X-gal stained tails were refixed in 3.7% formaldehyde/PBS, the caudal vertebral bones were demineralized in Plank–Rychlo solution and embedded in paraffin according to standard procedures. Sections of 8 μm were prepared and counterstained with Nuclear Fast red.

Construction and transfection of the *Skt* expression vector: To clone the full open reading frame (ORF) of the *Skt* gene, RT–PCR was performed using the Thermoscript RT–PCR system. The initial PCR was performed using the primer ORFS1 in the sense strand upstream from the start codon in the *Skt* gene (5'-ACCGGAGTGGAGACTAGTTG-3') and primer ORFA1 in the antisense strand downstream from the stop codon in the *Skt* gene (5'-TGCATGAGGCCTTGAACGATACAG-3'). Then, nested PCR was performed using the sense-strand primer ORFS2 (5'-TTTCTGCGAGCTTTCCGAAC-3') and the antisense-strand primer ORFA2 (5'-ACCTTGGTCCTAATAGGATCTG GC-3'). The PCR conditions used were 94° for 1 min, 58° for 1 min, and 72° for 3 min using 1.0 unit of LA Taq polymerase (Takara Biomedicals) for 25 cycles. The 4.1-kb PCR products were cloned into the pGEM-T vector (Promega, Madison, WI). This cDNA ORF was confirmed by sequencing and cloned into the pCAGGS expression vector (NIWA *et al.* 1991). Transfection into BMT10 cells (GERARD and GLUZMAN 1985) was carried out by the lipofection method using LipofectAMINE reagent (Invitrogen).

Western blot analysis: BMT10 cells and 40 pieces of the nucleus pulposus of caudal IVDs of adult mice were homogenized in 2× sample buffer (100 mM Tris HCl pH 6.8, 4% SDS,

12% β-mercaptoethanol, 20% glycerol). Extracts were electrophoresed on a 6.0% polyacrylamide gel, transferred to a nitrocellulose filter (Immobilon, Millipore, Bedford, MA), and detected using anti-Skt antibodies with the ECL detection system (Amersham, Arlington Heights, IL).

Immunohistochemistry: Tails were fixed in 4% paraformaldehyde in PBS. The caudal vertebral bones were demineralized in 0.24 M EDTA-2Na, 0.22 M EDTA-4Na solution for 48 hr and embedded in paraffin blocks. Sections of the IVDs were immunostained with anti-Skt antibodies by the avidin–biotin complex method (Vector Laboratories, Burlingame, CA). Sections were counterstained with hematoxylin.

RESULTS

Generation of *Sickle tail* mutant mice: A gene-trap ES clone was isolated by the exchangeable gene-trap method using the trap vector pU-8 (ARAKI *et al.* 1999). We obtained eight chimeric mice of which three were germline chimeras. Heterozygous animals appeared normal and were fertile. About half (35/66) of the homozygotes, however, showed a peculiar kinky-tail phenotype (Figure 1A and Table 1). This mutant mouse line was designated as B6;CB-*Skt^{GtAyu8021Imeg}*, in which *Skt* means *Sickle tail* because of the characteristic shape of the tail. Shortened and curved caudal vertebrae were apparent by the age of 2 weeks and were restricted to the 20–25th caudal vertebrae (Figure 1B). In contrast, heterozygous *Sd* mice showed short tails with truncation of vertebral columns at the 6th caudal vertebral body on average (Figures 1B and 7A) as reported previously. In *Skt^{Gt/Gt}* mice, no other skeletal abnormality was observed by bone X-ray examination (data not shown).

TABLE 1

Summary of genotyping of 4-week-old mice from *Skt^{Gt}* heterozygote matings

		Gt/Gt	
+/+	Gt/+	Kinked	Normal[a]
60	151	35 (53%)	31

[a] All normal-looking homozygotes showed deformity of the caudal discs by histological analysis.
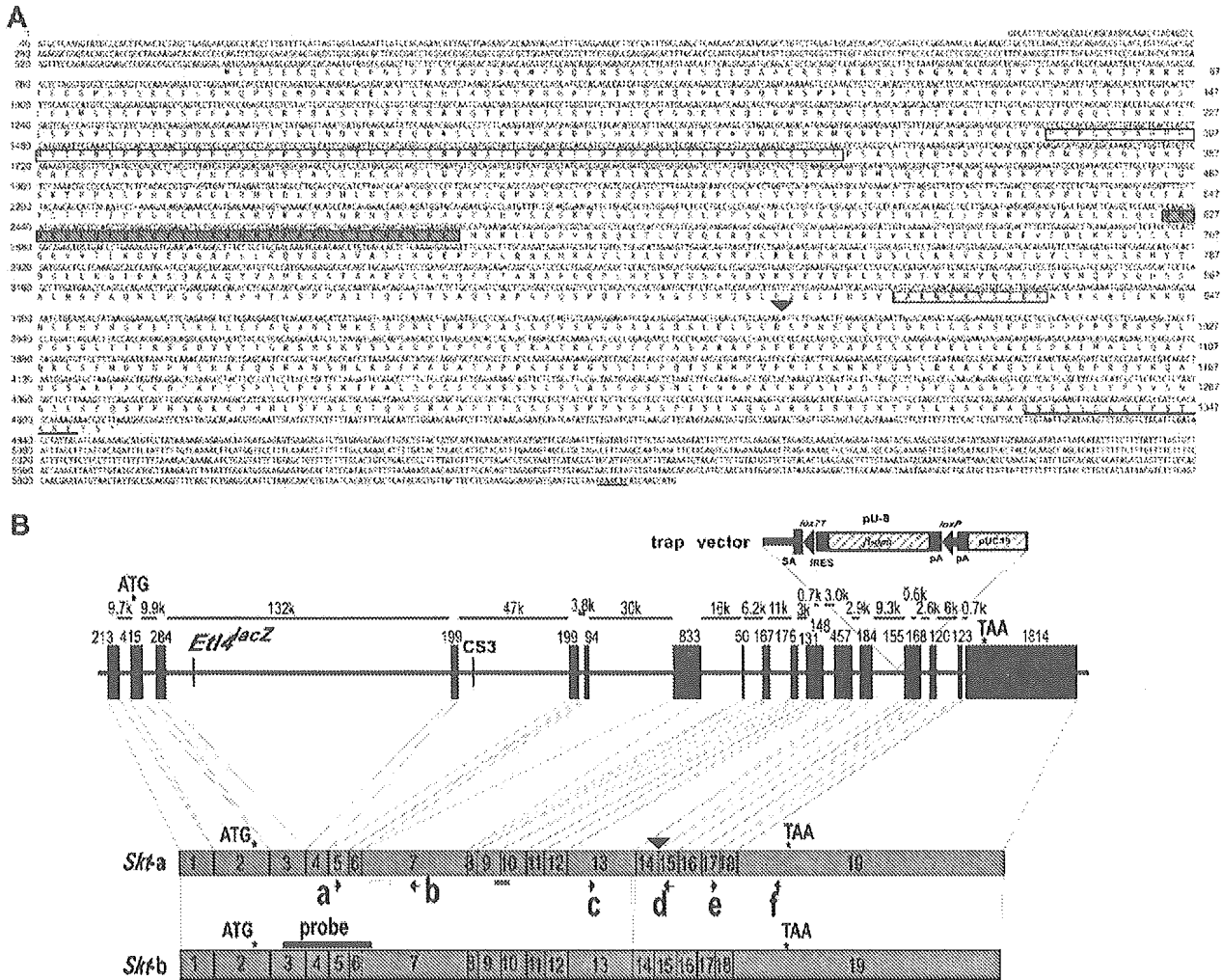
A

B

FIGURE 2.—Identification of the trapped gene *Skt*. (A) The nucleotide sequence of the *Skt* cDNA and predicted amino acid sequence. The open box indicates the pro-rich region at the N terminus and the shaded box indicates the coiled-coil region in the middle. The striped box indicates the sequence deleted in *Skt*-b by alternative splicing. The 15-amino-acid peptide used for the production of anti-Skt antibodies is shown by underlining. The polyadenylation signal is underlined at the 3'-end of the nucleotide sequence. The nucleotide sequence is numbered on the left side and the amino acid sequence is numbered on the right side. (B) Genomic structure of the *Skt* gene. (Top) Exon-intron structure of the *Sickle tail* gene. The trap vector, pU-8, was inserted into the 14th intron. Sizes of exons and introns are given. (Bottom) Two transcripts produced from the *Skt* allele. There are at least two types of *Skt* transcripts: one contains all the exons (termed *Skt*-a) and the other lacks 33 bp of the 13th exon (termed *Skt*-b). Arrows (a–f) indicate the location of the primers used for RT–PCR analyses in Figure 3, A–C, to detect the expression of each part of the *Skt* transcripts. The solid bar represents a probe used for Northern blotting. The open and shaded boxes indicate the pro-rich region and the coiled-coil region, respectively. The start and stop codons of the *Skt* gene are shown by asterisks. A sequence with high homology to the CS3 in node/notochord enhancers is located in the fourth intron of the *Skt* gene 106 kb downstream of the insertion site of *Etl4*[*lacZ*].

Characterization of the integration site of the trap vector: To characterize the gene-trap locus, we cloned and sequenced genomic DNA fragments flanking the gene-trap vector. A single copy of the vector was integrated into the genome as determined by Southern blot analysis using genomic DNA samples extracted from *Skt*[*a*] mice. Three base pairs of genomic DNA were deleted at the integration site of the trap vector. Using PCR amplification on genomic DNA samples, the genotype of offspring from the heterozygous intercross was easily determined (data not shown).

Identification of the *Sickle tail* gene: To identify the gene trapped, we performed 5'-and 3'-RACE. The sequence of the ORF of the trapped gene was determined by compiling sequences of 5'- and 3'-RACE products and of EST that showed 100% homology to the RACE products. We thus obtained a cDNA sequence comprising 5930 nucleotides (accession no. AB125594) that encodes a putative protein of 1352 amino acids with a predicted molecular weight of 147 kDa (Figure 2A). This gene was termed *Skt*. The protein contains a proline-rich region (amino acid residues 298–364) and a coiled-coil region